Mechanism-Guided Design and Discovery of Efficient Cytochrome P450-Derived C—H Amination Biocatalysts

Viktoria Steck[‡], Joshua N. Kolev[‡], Xinkun Ren, and Rudi Fasan*

Department of Chemistry, University of Rochester, Rochester, NY 14627, United States.

ABSTRACT: Cytochromes P450 have been recently identified as a promising class of biocatalysts for mediating C—H aminations via nitrene transfer, a valuable transformation for forging new C—N bonds. The catalytic efficiency of P450s in these non-native transformations is however significantly inferior to that exhibited by these enzymes in their native monooxygenase function. Using a mechanism-guided strategy, we report here the rational design of a series of $P450_{BM3}$-based variants with dramatically enhanced C—H amination activity acquired through disruption of the native proton relay network and other highly conserved structural elements within this class of enzymes. This approach further guided the identification of XplA and BezE, two 'atypical' natural P450s implicated in the degradation of a man-made explosive and in benzastatins biosynthesis, respectively, as very efficient C—H aminases. Both XplA and BezE could be engineered to further improve their C—H amination reactivity, which demonstrates their evolvability for abiological reactions. These engineered and natural P450 catalysts can promote the intramolecular C—H amination of arylsulfonyl azides with over 10,000-14,000 catalytic turnovers, ranking among the most efficient nitrene transfer biocatalysts reported to date. Mechanistic and structure-reactivity studies provide insights into the origin of the C—H amination reactivity enhancement and highlight the divergent structural requirements inherent to supporting C—H amination versus C—H monooxygenation reactivity within this class of enzymes. Overall, this work provides new promising scaffolds for the development of nitrene transferases and demonstrates the value of mechanism-driven rational design as a strategy for improving the catalytic efficiency of metalloenzymes in the context of abiological transformations.

KEYWORDS: Cytochrome P450, C—H amination, nitrene transfer, kinetic isotope effects, sulfonyl azides, isotopically sensitive branching.

Introduction

The functionalization of C(sp^3)—H bonds is a fundamentally useful transformation in organic chemistry as it enables the rapid construction of organic molecules and increases the efficiency of chemical syntheses.[1-5] Of particular interest is the selective amino functionalization of C—H bonds owing to the ubiquitous presence of amine functionalities in synthetically valuable and biologically active compounds. Major advances in this area have led to the development of organometallic catalysts for catalyzing the insertion of nitrene species into C—H bonds.[6-11] Recently, our group and others have reported that cytochromes P450,[12-14] cytochromes P411,[15-20] and other hemoproteins[21-22] are capable of engaging organic azides or other nitrene precursors in nitrene transfer reactions. These include intra- and intermolecular C—H aminations,[12-13,15,18-21] sulfimidation,[16] aziridination,[17] and other transformations.[14,22] In this context, our group demonstrated that an engineered variant of the bacterial fatty acid hydroxylase $P450_{BM3}$, called FL#62, is capable of promoting an intramolecular C(sp^3)—H amination reaction with arylsulfonyl azides to yield benzosultams, supporting up to ~400 catalytic turnovers (TON).[12] Arnold and co-workers reported a comparable activity (~360 TON) for serine-ligated $P450_{BM3}$ variants in the same reaction,[15] and a similar performance was observed for artificial P450 metalloenzymes harboring an abiological Ir(Me) mesoporphyrin IX cofactor (~300 TON).[23] While the catalytic activity of these engineered P450s in C—H amination reactions exceeds that of synthetic catalysts (typically, <100-150 TON), this reactivity remains far below that achievable by these enzymes in monooxygenation reactions, some of which have been reported to exceed 60,000 total turnovers.[24-36]

In previous work, we proposed a plausible mechanism for P450-catalyzed C—H amination reactions,[12-13] which involves an initial reduction of the hemoprotein via NADPH or an exogenous reductant (i.e., sodium dithionite) to give the catalytically active ferrous form of the enzyme (**Figure 1A**). The organic azide substrate is envisioned to bind to the iron center resulting in a heme-azide complex, which, upon nitrogen extrusion, leads to the formation of a putative iron-nitrenoid intermediate.[12] Via experiments with radical probe substrates, we further established that the C—H amination reaction proceed via a stepwise, H atom abstraction/radical rebound mechanism (**Figure 1A**, productive pathway (blue)).[13]

The latter was further supported by more recent computational (DFT) analyses[37] and studies on P450-catalyzed C—H aminations with other nitrene precursors.[20] Along with the productive pathway mentioned above, an unproductive pathway involving protonation and reduction of the putative iron-nitrenoid intermediate was proposed to account for the accumulation of reduced sulfonamide byproduct in the reactions with sulfonylazide substrates (**Figure 1A**, nonproductive pathway (grey)).[12-13] This competing side reaction, which has been observed in various other hemoprotein-catalyzed nitrene transfer reactions,[13,17] inherently reduces the catalytic efficiency of these biocatalysts in the context of these non-native transformations. Guided by mechanistic considerations concerning the origin of this nonproductive pathway, we report here the rational design of engineered P450-based catalysts with greatly increased C—H amination efficiency via targeting and altering a series of conserved structural elements present in these enzymes. In addition, this mechanism-driven approach led to the discovery of two naturally occurring P450s, XplA and BezE, as efficient C—H aminases, thereby providing additional metalloprotein scaffolds for the development of novel nitrene transfer biocatalysts.

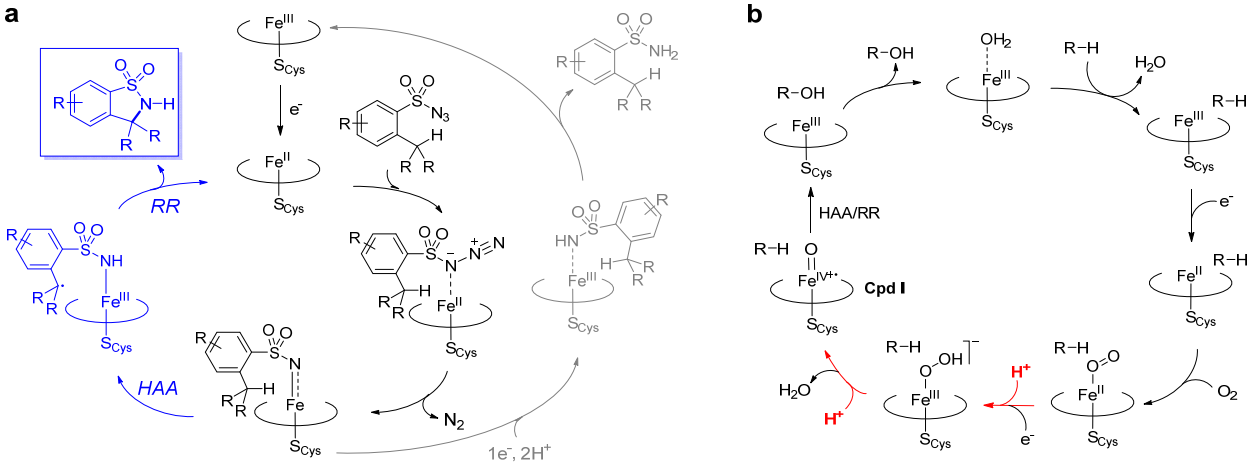

Figure 1. **C—H amination vs. C—H hydroxylation mechanism.** (A) Proposed mechanism for cytochrome P450-catalyzed C—H amination of sulfonyl azides (*blue*) and the unproductive pathway leading to sulfonamide formation (*grey*). HAA = H atom abstraction; RR = radical rebound. (B) Catalytic cycle for P450-catalyzed monooxygenation (hydroxylation). The two proton transfer steps implicated in the formation of Compound I (Cpd I) are highlighted in red.

Results and Discussion

Mutagenesis of Proton Relay Residues

The proposed mechanism for P450 catalyzed C—H amination (**Figure 1A**) differs significantly from the canonical monooxygenation mechanism of cytochromes P450 (**Figure 1B**).[38] In the native monooxygenation reaction, upon formation of the iron-peroxo intermediate, two proton transfers along with two single-electron transfers (SET) are required for the heterolytic cleavage of the O—O bond, leading to the formation of Compound I ((heme)Fe(IV)=$O^{\bullet+}$) as the active oxidant species (**Figure 1B**). Because of the functional importance of these proton transfer steps for monooxygenation reactivity, a highly conserved threonine (or serine) residue is found in the I helix of P450s (**Figures 2a**), which is implicated in the delivery of protons to the distal oxygen of the iron-peroxide intermediate leading to heterolytic cleavage of the O—O bond to form Compound I.[39-41] Consistent with its role in facilitating the formation of Compound I, mutation of this residue has been associated with a decrease in coupling efficiency and monooxygenation activity in P450s.[39-41] While this conserved threonine residue is critical for monooxygenase activity, we hypothesized that the proton transfer process mediated by this residue and associated proton relay pathway (*vide infra*) is not only unnecessary but actually deleterious in the context of the non-native C—H amination reactivity, potentially contributing, at least in part, to the unproductive reductive pathway occurring in P450-catalyzed nitrene transfer reactions and thus to reducing the efficiency of these processes. Accordingly, we surmised that disruption of the native proton relay system could provide a pathway to develop more efficient P450-based C—H amination catalysts.

To test this approach, we selected as model system the intramolecular C—H amination of sulfonyl azides catalyzed by FL#62, an engineered variant of the bacterial long-chain fatty acid hydroxylase $P450_{BM3}$ we previously identified to exhibit good activity in this reaction.[12] In this P450, the highly conserved threonine residue lying above the heme cofactor corresponds to Thr268 (**Figure 2a**).[41] As this residue is buried in the core of the enzyme, a more extended proton relay network must be involved in shuttling protons from the bulk solvent to the heme-bound oxygen and hydroperoxo species during the native catalytic cycle for monooxygenation (**Figure 1b**). Upon inspection of $P450_{BM3}$ crystal

structure,[42] we identified His266, Glu267, and Thr438 as potential residues involved in this proton shuttle pathway, based on the H-bonding ability of their side-chain groups and close distance from each other and from Thr268 (**Figure 2a**). In $P450_{cam}$, an aspartate residue (Asp251) corresponding to Glu267 in $P450_{BM3}$ was previously suggested to operate in concert with the conserved threonine (Thr252 in $P450_{cam}$) in the aforementioned proton transfer process.[43]

Following the mechanistic considerations outlined above, Thr268, His266, Glu267, and Thr438 were targeted for mutagenesis with the purpose of disrupting the native proton relay network in this P450. To this end, His266, Thr268, and Thr438 were substituted for the isosteric yet non-hydrogen bonding amino acids Phe and Val, respectively, in order to remove their proton transfer ability without altering the steric environment around the active site. Glu267 was mutated to alanine as its side chain is solvent exposed and thus unlikely to have an impact on substrate orientation within the active site. The corresponding single-site FL#62 variants were then tested for their C—H amination activity using the model substrate 2,4,6-triisopropylbenzenesulfonyl azide **1a** (**Table 1**, Entries 2-6). These reactions were carried out under catalyst-limited conditions (i.e., by measuring total turnovers or TTN), to best assess the effect of the mutations on the enzyme catalytic efficiency in this reaction. Gratifyingly, all of these rationally designed variants with the only exception of FL#62(E267A), were found to exhibit a significant increase in C—H amination activity over the parent protein FL#62. Among them, FL#62(H266F) and FL#62(T268V) were identified as the most active variants, supporting ~1,700 TTN for the formation of **1b** compared to 460 TTN for the parent enzyme (**Table 1**, Entries 2 and 5 vs. 1). Interestingly, the isosteric T268V mutation shows a more beneficial effect compared to a T268A mutation previously introduced in this enzyme (1,640 vs. 1,210 TTN; Entry 5 vs. 4).[12]

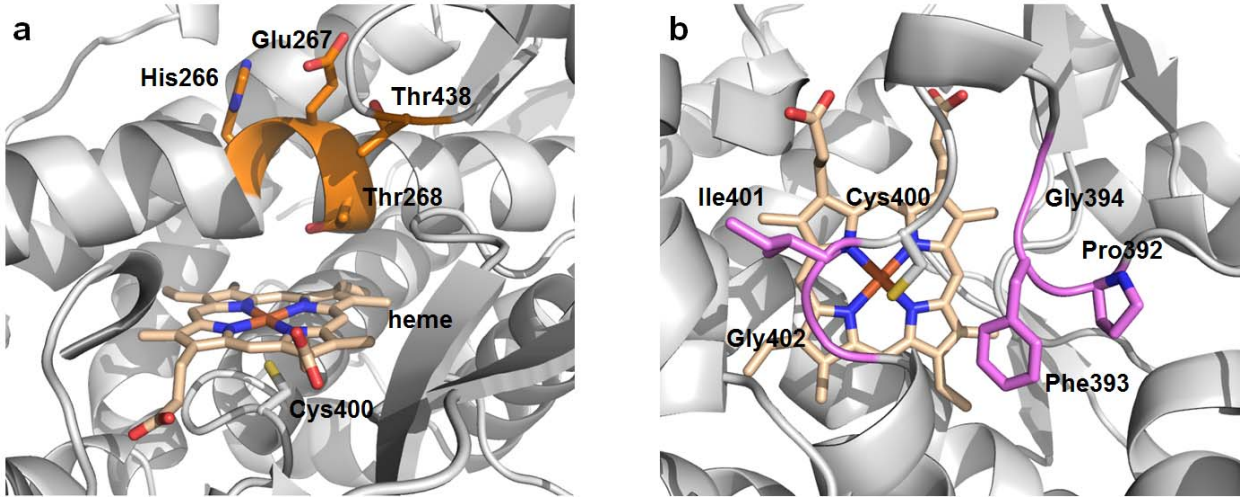

Figure 2. Distal and proximal regions surrounding the heme cofactor (stick model, wheat) in the crystal structure of cytochrome $P450_{BM3}$ heme domain (pdb 1BU7). A) View of the $P450_{BM3}$ heme pocket highlighting Thr268 and other putative proton relay residues targeted by mutagenesis (orange). B) View of proximal region of the enzyme highlighting the cysteine-ligand loop residues and other nearby residues targeted for mutagenesis (purple). The heme-ligating cysteine residue is also shown as stick model (grey).

These results encouraged us to combine the mutations H266F, E267A, T268V, and T438V to give a series of double and triple mutant variants (**Table 1**, Entries 7-11). Among these second-generation variants, FL#62(H266F,T268V) emerged as the best catalyst, supporting 2,450 TTN for the C—H amination of **1a** (**Table 1**, Entry 7). Introduction of the beneficial T438V mutation in FL#62(H266F,T268V) (**Table 1**, Entry 11) did not yield further increases in activity. Similarly, pairing the E267A mutation with the beneficial mutations T268V or T438V led to catalysts with C—H amination activity comparable or lower than that of the single variants (**Table 1,** Entries 8-9). Overall, the beneficial effect of the rationally designed mutations along with the additive effect of the H266F and T268V mutations supported our working hypothesis that targeting the native proton relay pathway is beneficial toward enhancing the C—H amination reactivity of this P450.

Table 1. Catalytic turnovers and selectivity of engineered P450$_{BM3}$ catalysts for the C—H amination of 2,4,6-triisopropylbenzenesulfonyl azide **1a**.[a]

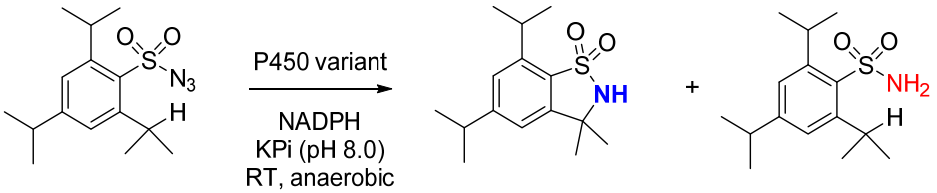

1a **1b** **1c**

Entry	Variant	TTN[b]	Select. (%)[c]
1	FL#62	460 ± 15	86%
2	FL#62(H266F)	1,700 ± 90	88%
3	FL#62(E267A)	340 ± 30	77%
4	FL#62(T268A)	1,070 ± 35	86%
5	FL#62(T268V)	1,640 ± 160	88%
6	FL#62(T438V)	1,210 ± 50	89%
7	FL#62(H266F,T268V)	2,450 ± 300[d]	87%
8	FL#62(E267A,T268V)	1,680 ± 250	89%
9	FL#62(E267A,T438V)	360 ± 30	84%
10	FL#62(T268V,T438V)	640 ± 120	85%
11	FL#62(H266F,T268V,T438V)	2,170 ± 75[d]	82%
12	FL#62(H266F,T268V,P392G)	3,360 ± 150[d]	87%
13	FL#62(H266F,T268V,F393P)	2,650 ± 300[d]	81%
14	FL#62(H266F,T268V,G394P)	2,430 ± 50[d]	75%
15	FL#62(H266F,T268V,I401P)	1,260 ± 90[d]	79%
16	FL#62(H266F,T268V,G402P)	2,630 ± 290[d]	71%
17	FL#62(H266F,T268V,P392G)	14,800 ± 800[e]	74%

[a] 0.5 µM P450, 3 mM substrate, 10 mM NADPH, 50 mM potassium phosphate buffer (pH 8.0), 16 hours. [b] Total number of catalytic turnovers (mol sultam mol^{-1} P450). SD values are from triplicate experiments. [c] Mol sultam (**1b**) / mol total products (**1b** + **1c**). [d] 10 mM substrate. [e] *E. coli* cells expressing P450 variant at OD_{600} = 40, 10 mM substrate, 50 mM potassium phosphate buffer (pH 7.2), 16 hours.

Alteration of the heme environment

More broadly, the studies above suggested to us that altering conserved structural elements in a P450 can help improve its non-native nitrene transferase activity. Indeed, further characterization of FL#62(H266F,T268V) revealed that its CO-bound form exhibits a Soret band with a λ_{max} at 422 nm (**Figure 3b**) instead of the typical 450 nm peak (**Figure 3a**), a spectroscopic feature characteristic of cytochromes P450 with a folded structure but an altered heme ligation environment.[44-46] Based on these considerations, we sought to further improve the catalytic performance of these engineered P450 variants by targeting other conserved structural features around the heme group, namely the loop encompassing the invariable heme-ligating cysteine residue (C400) and other conserved residues lying underneath the heme cofactor (**Figures 2b** and **S1**). We envisioned that amino acid mutations targeted to this region of the protein could lead to a perturbation of the heme environment, potentially resulting in increased nitrene transfer reactivity. Accordingly, mutations P392G, F393P, G394P, I401P, and G402P were introduced into the best 'proton relay variant', FL#62(H266F,T268V), to give a series of triple mutants. In this case, a Xaa→Pro and Pro→Gly mutagenesis strategy was applied with the goal of inducing a significant conformational change at the level of each of these residues (**Figure 2b**). This approach led to P450 variants with improved catalytic activity in the C—H amination of **1a** compared to FL#62(H266F,T268V) (**Table 1**, Entries 12-16). In particular, FL#62(H266F,T268V,P392G) was identified as the most active C—H aminase within this third generation of variants, supporting 3,360 TTN for this reaction *in vitro*. Notably, this P450 variant was found to display a significantly altered spectroscopic profile compared to canonical P450s (**Figure 3a**), showing a weak and blue shifted Soret band at 383 nm in its ferric state and a weak band with a maximum absorption at 422 nm in its CO-bound form (**Figure 3c**). These features are clearly indicative of a major structural distortion at the level of protein-bound heme cofactor induced by the P392G mutation, causing the protein to lose its characteristic P450s features.

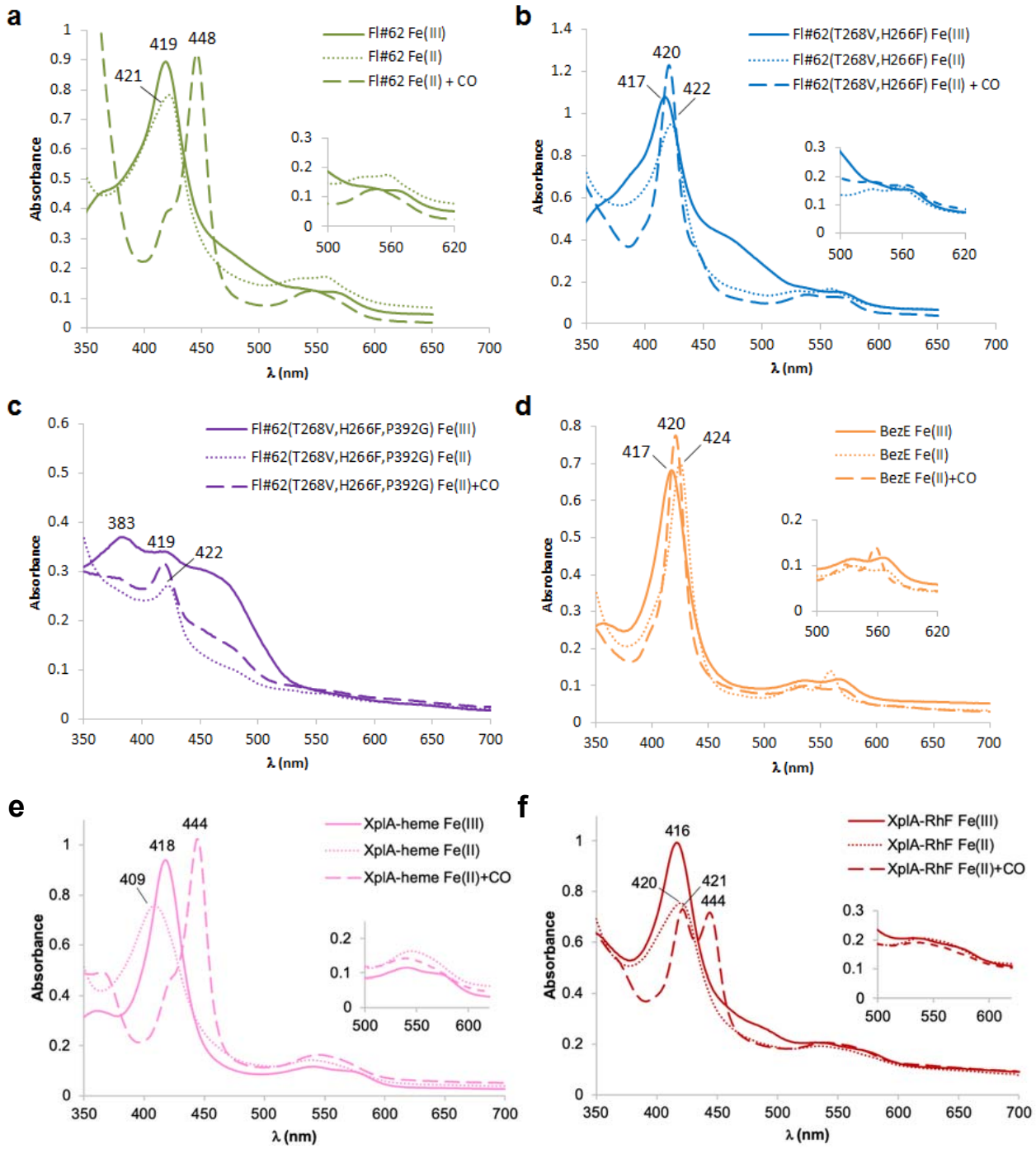

Figure 3. Electronic absorption spectra for (a) FL#62, (b) FL#62(H266F,T268V), (c) FL#62(H266F,T268V,P393G), (d) BezE, (e) XplA-heme and (f) XplA-RhF in their ferric (solid line), ferrous (dotted line), and CO-bound form (dashed line). The insert shows the Q band region.

Further characterization via kinetic experiments showed that the increase in catalytic activity (TTN; **Table 1**) exhibited by the improved FL#62-derived C—H aminases is accompanied by an increase in their catalytic efficiency (k_{cat}/K_M) for the C—H amination reaction (**Table 2**). A 2- and 3-fold higher k_{cat}/K_M value was indeed measured for FL#62(T268V) and FL#62(H266F), respectively, compared to the parent enzyme FL#62 (k_{cat}/K_M = 128-193 $M^{-1}s^{-1}$ vs. 56 $M^{-1}s^{-1}$), with this increase in catalytic efficiency being mostly driven by a decrease in K_M. The combination of the beneficial T268V and H266F mutations resulted in nearly additive improvement in catalytic efficiency (k_{cat}/K_M = 295 $M^{-1}s^{-1}$) for the intramolecular C—H amination of **1a**, corresponding to a five-fold enhancement over FL#62. A similar increase in k_{cat}/K_M is also displayed by FL#62(H266F,T268V,P393G), whose improvement in catalytic efficiency is mainly driven by an increase in the turnover number (k_{cat} = 3.4 s^{-1} vs. 0.96 s^{-1} for FL#62; **Table 2**). To further assess the catalytic efficiency of FL#62(H266F,T268V,P329G), this variant was tested in whole-cell biotransformation with **1a**. Under these conditions, this variant was found to produce the desired sultam product **1b** in 70% yield with a TTN value of 14,800 (**Table 1**, Entry 17). This TTN value corresponds to the highest catalytic activity for a biocatalytic nitrene transfer reaction reported to date, with only one notable exception[20], and it compares well with the highest TTN values reported for monooxygenation reactions catalyzed by engineered P450s.[24-36]

Table 2. Kinetic parameters of the different P450-derived catalysts for the intramolecular C—H amination of **1a** into sultam **1b**.[a]

Entry	Catalyst	K_M (mM)[b]	k_{cat} (s^{-1})[b]	k_{cat}/K_M (M^{-1} s^{-1})
1	FL#62	17.0 ± 2.7	0.96 ± 0.14	56 ± 12
2	FL#62(H266F)	1.4 ± 0.2	0.27 ± 0.06	193 ± 50
3	FL#62(T268V)	3.9 ± 0.1	0.50 ± 0.03	128 ± 8
4	FL#62(H266F,T268V)	2.0 ± 0.2	0.59 ± 0.05	295 ± 38
5	FL#62(H266F,T268V,P392G)	12.2 ± 1.9	3.4 ± 0.4	280 ± 55
6	XplA-RhF	5.2 ± 1.2	1.1 ± 0.2	228 ± 67
7[c]	BezE	7.0 ± 0.9	14.7 ± 0.4	2,140 ± 280

[a] Conditions: 1 μM P450, 0.5 mM to 10 mM substrate, 10 mM NADPH, 50 mM potassium phosphate buffer, pH 8.0. Reaction were quenched at 5 min after addition of substrate. [b] Derived from Michaelis Menten equation; reported value are mean ± SD. [c] Using 10 mM $Na_2S_2O_4$, 50 mM potassium phosphate buffer, pH 6.0.

Analysis of C—H amination reactivity and selectivity

To determine whether the improved activity of the P450 variants toward **1a** reflects a general enhancement in the C—H amination reactivity of these enzymes, FL#62(H266F,T268V) and FL#62(H266F,T268V,P393G) were tested against a broader panel of sulfonyl azide substrates (**Figure 4a**). Across all these substrates, both variants displayed a significant improvement in catalytic activity compared to the parent enzyme. These improvements corresponded to a 5-fold to 10-fold increase in total turnovers for the cyclization of compound **3a** and **4a**. An even larger activity improvement (87-fold) was observed for the cyclization of **2a** catalyzed by FL#62(H266F,T268V,P393G), which supports 870 TTN in this reaction compared to only 10 TTN for FL#62 (**Figure 4a**). Further corroborating this trend, a good overall correlation ($R^2 = 0.61$) was found across the entire set of engineered FL#62-derived variants between their TTN toward the synthesis of **2b** vs. **1b** (**Figure 4b**). Altogether, these results demonstrated that the improved performance of

these biocatalysts is not limited to the substrate utilized during the initial activity studies, but it rather reflects a general enhancement of their catalytic efficiency as nitrene transferases.

As the mutations in the 'proton relay variants' series were designed to suppress the unproductive pathway leading to the reduction (sulfonamide) byproduct, we then investigated the selectivity of these P450s with respect to formation of the C—H amination over the reduction byproduct using 2,4,6-triethylbenzenesulfonyl azide **4a** as the probe substrate. Unlike for **1a**, the FL#62-catalyzed C−H amination of **4a** proceeds with modest selectivity (17% vs. 86%), indicating that the unproductive reductive pathway competes significantly with the C—H amination pathway in this substrate. This also corresponded to a significantly lower efficiency of this enzyme toward cyclization of **4a** vs. **1a** (34 vs. 460 TTN). Importantly, these experiments revealed that the large majority of the proton relay variants, and in particular FL#62(H266F,T268V) and FL#62(H266F,T268V,T438V), exhibit an improvement in the selectivity of the reaction (28-31%) compared to the parent enzyme FL#62 (17% select.) (**Table S1**). Overall, these results are consistent with the notion that the introduced mutations are effective toward suppressing the unproductive pathway leading to the reduction byproduct, thereby resulting in an increased C—H amination efficiency.

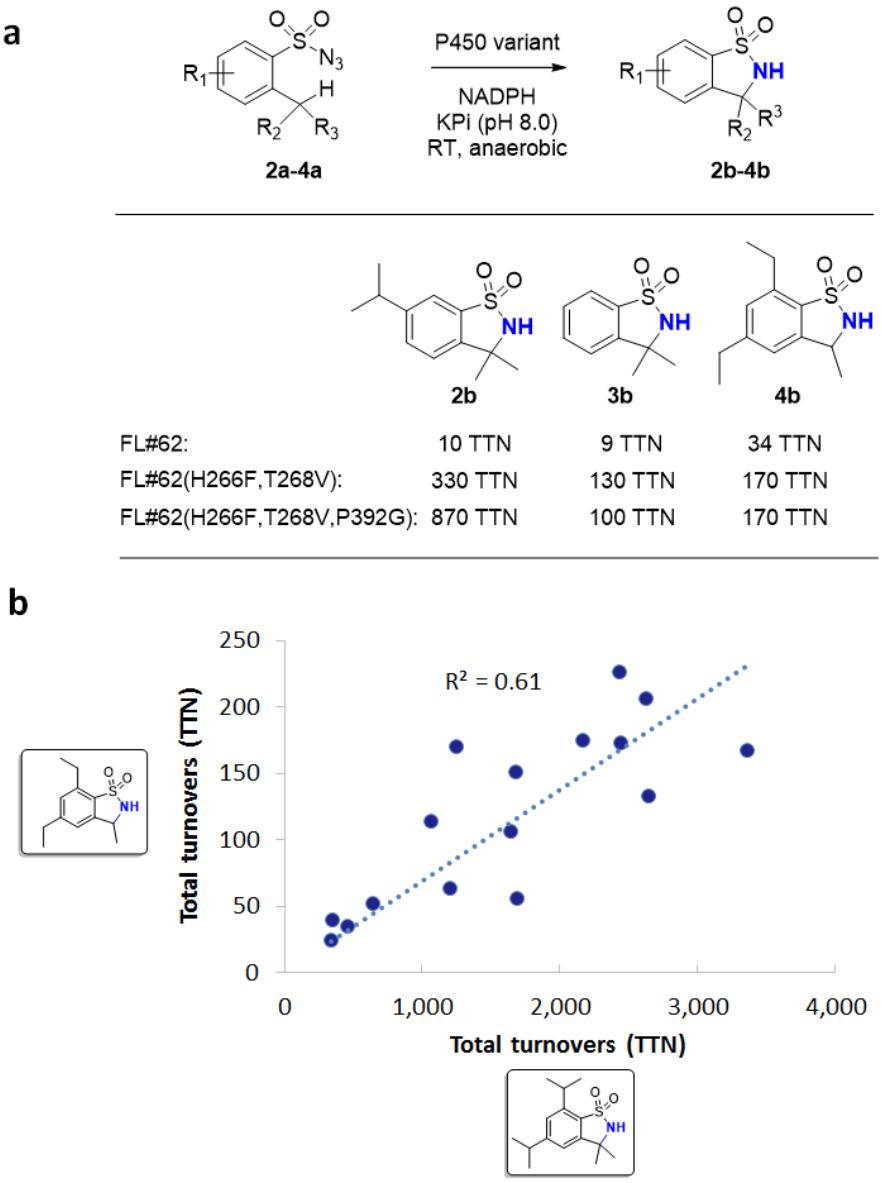

Figure 4. C—H amination activity of panel of FL#62-derived variants on differently substituted arylsulfonyl azides **2a-4a** (a) and correlation between their TTN values for the C—H amination of **1a** and **4a** (b).

Monooxygenase Activity of Improved C—H Aminases

To examine the impact of these mutations on the native monooxygenase activity of the P450s, the improved C—H aminases were further characterized with respect to their hydroxylation activity on methyl ibuprofen (mIbu. **5**), a small-molecule drug previously found to be a viable substrate for oxidation by engineered $P450_{BM3}$ variants.[31,47] FL#62 catalyzes

the hydroxylation of mIbu to yield **6** and **7** in a 91:9 ratio with 1,100 TTN (**Table 3**). In contrast, FL#62(H266F,T268V) showed a significantly reduced efficiency toward this monooxygenation reaction, supporting 186 TTN (= 83% reduction in activity). Moreover, the further improved C—H aminase FL#62(H266F,T268V,P392G) was nearly inactive as monooxygenase, displaying only 5 TTN in this reaction and thus a >99% drop in activity compared to FL#62. A similar trend was observed for the product formation rate in these hydroxylation reactions, which decreased by 50- and >500-fold for FL#62(H266F,T268V) and FL#62(H266F,T268V,P392G), respectively, compared to the parent enzyme (**Table 3**). Similarly, the coupling efficiency of the P450s was found to drop from 74% for FL#62 to 25% for FL#62(H266F,T268V) and to less than 1% for FL#62(H266F,T268V,P392G). The significantly increased uncoupling of the latter P450 variants in the monooxygenation reaction is consistent with an impairment of the proton transfer steps implicated in P450 catalytic cycle as monooxygenase,[39-41] thus further supporting the predicted role of the mutations in altering the native proton transfer mechanisms in these enzymes. Overall, the inverse correlation between the C—H amination and C—H hydroxylation activity across this panel of P450 variants highlighted the fact that divergent, and nearly orthogonal, active site features are critical for supporting the non-native nitrene transfer reactivity compared to the native monooxygenase activity.

Table 3. Hydroxylation activity of engineered P450$_{BM3}$ C—H amination catalysts on ibuprofen methyl ester (**5**).[a]

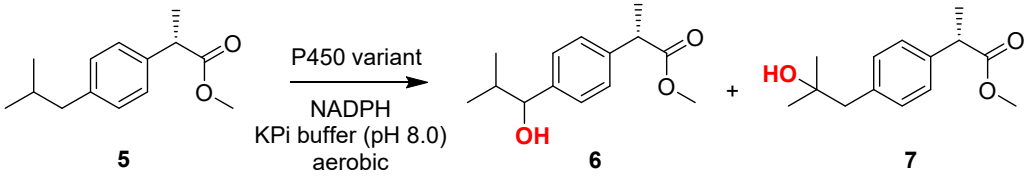

5 **6** **7**

Variant	TTN[b]	**6**	**7**	Rate[c] (TON min^{-1})	Coupling Efficiency[d]
FL#62	1,100 ± 80	91%	9%	1,230 ± 35	74%
FL#62 (H266F,T268V)	185 ± 15	91%	9%	25 ± 1	25%
FL#62 (H266F,T268V,P392G)	5 ± 1	79%	21%	2 ± 0.2	<1%

[a] 0.1-1 μM P450, 1 mM mIbu (**5**), 2 μM phosphite dehydrogenase (PTDH), 100 μM $NADP^+$, 50 mM potassium phosphite in potassium phosphate buffer (50 mM, pH 8), 16 hours. [b] Total turnover numbers (mol (**6**+**7**) mol^{-1} P450). [c] Rate of product formation (turnovers min^{-1}) over initial 30 sec. [d] Ratio between rates of product formation and NADPH oxidation over initial 30 sec.

Naturally occurring P450 XplA and BezE are efficient C—H aminases

Motivated by these findings, we sought to identify naturally occurring P450s which could potentially support non-native nitrene transferase reactivity by virtue of their atypical active site features and/or catalytic properties. Following these guiding principles, we identified in the cytochrome P450 XplA from *Rhodococcus* sp.[48] and in the cytochrome P450 BezE from *Streptomyces* sp. RI18[49] two potential candidates for this purpose. XplA, which was isolated from an organism found in sites contaminated by the man-made explosive RDX (hexahydro-1,3,5-trinitro-1,3,5-triazine),[48] catalyzes the degradation of RDX to nitrite, 4-nitro-2,4-diazabutanal, formaldehyde and ammonia, which is used as a nitrogen source by the host organism (**Figure 5c**).[50-51] XplA is composed of a heme domain fused to a flavodoxin domain, which mediates the transfer of electrons from a cognate ferredoxin reductase (and NADH) to the heme domain during catalysis.[48,52] Interestingly, the crystal structure of XplA heme domain[53] reveals that while sharing a common P450 fold, this enzyme lacks the highly conserved threonine and glutamate pair implicated in the native proton transfer pathway found in canonical P450s. Indeed, these residues are replaced in XplA by an alanine and methionine residue, respectively, whose presence also induce a prominent kink in the I helix (**Figure 5a-b**).[53] While this unusual active site configuration has likely evolved to favor RDX-degrading activity, we envisioned it would be beneficial for supporting non-native nitrene transfer activity, as suggested by our results with the FL#62-based proton relay variants. As a second candidate, we elected the P450 BezE recently reported by Oshini and co-workers.[49] This P450 participates in the biosynthesis of benzastatins by catalyzing the cyclization of geranyl functionalized precursors to give an indoline and tetrahydroquinoline product. This transformation shares mechanistic similarities with the activation of N-acylcarbamates we previously reported in the context of the P450-catalyzed cyclization of carbonazidates[13] and it was proposed to involve a nitrene-heme intermediate[49] analogous to that previously proposed for the P450-catalyzed C—H

amination of sulfonyl azides.[12] These mechanistic similarities suggested to us that BezE could exhibit C—H amination reactivity.

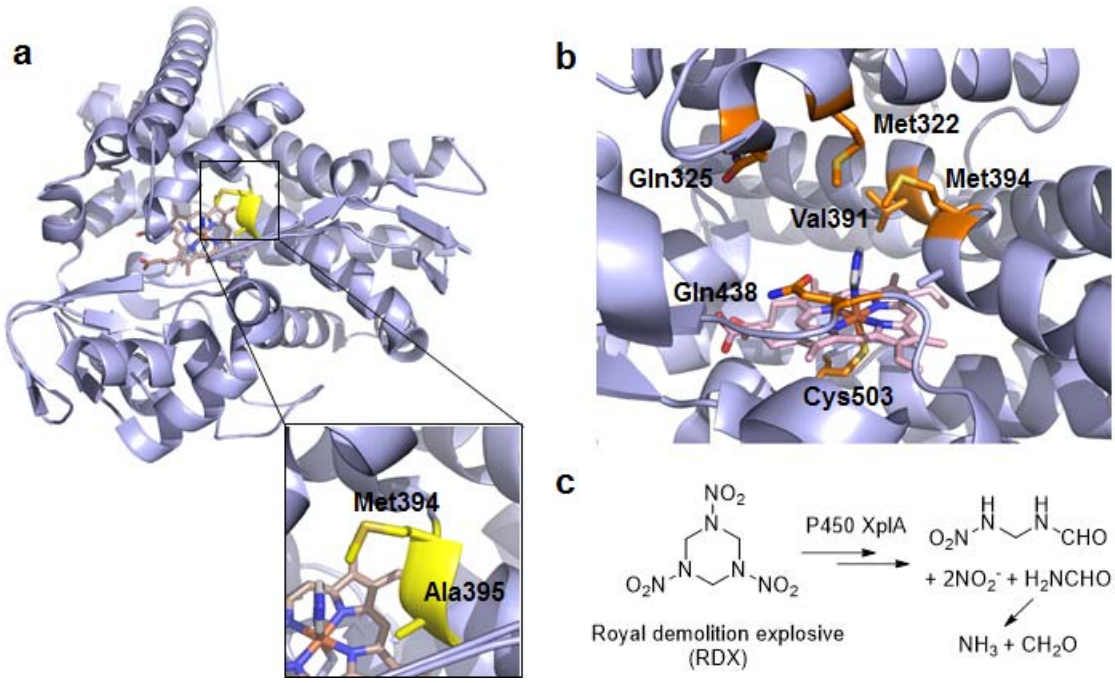

Figure 5. Crystal structure of XplA heme domain in complex with imidazole (pdb 4EP6). (a) Close-up view of the I helix region containing residues Met394 and Ala395 (stick models, yellow). (b) View of XplA heme pocket highlighting the active site residues targeted for mutagenesis (orange). (c) XplA-catalyzed catabolism of RDX.

Based on these considerations, the isolated heme domain of XplA ('XplA-heme') and BezE were tested for their ability to catalyze the C—H amination of 2,4,6-triisopropylbenzene-sulfonyl azide **1a** (**Table 4**). Both P450s were found to be able to catalyze this transformation with high efficiency. In particular, XplA was found to support over 1,700 TTN in this reaction with 82% selectivity for formation of the C—H amination product **1b** over the sulfonamide byproduct **1c** (**Table 4**, Entry 1). BezE also proved to be a remarkably efficient biocatalyst for this non-native reaction, supporting nearly 11,000 total turnovers for the formation of the C—H amination product in the presence of sodium dithionite as the reductant (**Table 4**, Entry 11). Thus, even prior to optimization via protein engineering, these natural P450 systems exhibit a C—H amination reactivity comparable

to that of the best performing FL#62-derived variants. In line with these results, kinetic experiments revealed that turnover rate (k_{cat}) and catalytic efficiency (k_{cat}/K_M) of XplA for the cyclization of **1a** are comparable to those of the best $P450_{BM3}$-derived C—H aminase FL#62(H266F,T268V,P392G) (**Table 2**, Entry 6 vs. 5). BezE, on the other hand, displays an even higher k_{cat} (14.7 s^{-1} vs. 3.4 s^{-1}) and k_{cat}/K_M values (2,140 $M^{-1}s^{-1}$ vs. 280 $M^{-1}s^{-1}$) (**Table 2**, Entry 7). Notably, the catalytic efficiency of BezE in this non-native reaction is comparable to that of certain biosynthetic P450s on their native reactions (~500-17,000 $M^{-1}s^{-1}$).[54-56]

Table 4. Catalytic activity and selectivity of wild type XplA and BezE and engineered variants thereof the in intramolecular C—H amination reaction with **1a**.[a]

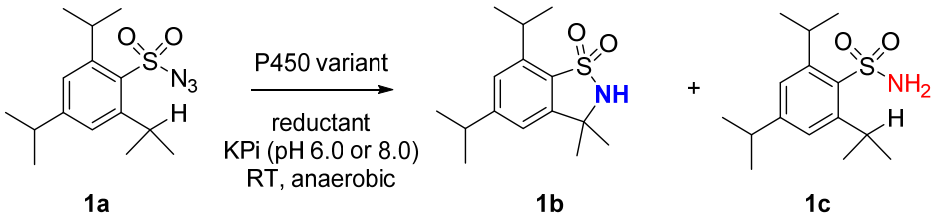

1a **1b** **1c**

Entry	Variant	Reductant	TTN[b]	Selectivity[c]
1	XplA-heme	$Na_2S_2O_4$	1,780 ± 170	82%
2	XplA-heme(M322A)	$Na_2S_2O_4$	1,710 ± 210	84%
3	XplA-heme(Q325A)	$Na_2S_2O_4$	2,890 ± 300	90%
4	XplA-heme(V391A)	$Na_2S_2O_4$	390 ± 45	92%
5	XplA-heme(M394A)	$Na_2S_2O_4$	380 ± 50	92%
6	XplA-heme(Q438A)	$Na_2S_2O_4$	610 ± 80	83%
7	XplA-heme(C503S)	$Na_2S_2O_4$	3,830 ± 120	87%
8	XplA-RhF	NADPH	8,090 ± 1270	96%
9	XplA-RhF	NADPH	5,460 ± 200[d]	91%
10	XplA-RhF	NADPH	13,410 ± 3600[e]	81%
11	BezE	$Na_2S_2O_4$	10,880 ± 1270	87%
12	BezE(T256V)	$Na_2S_2O_4$	11,200 ± 1280	86%

[a] 0.5 μM P450, 10 mM substrate, 10 mM reductant in 50 mM potassium phosphate buffer (pH 6.0 (BezE) or 8.0 (XplA)), 16 hours. [b] Total turnover numbers (mol sultam

mol^{-1} P450). [c] Mol sultam (**1b**) / mol total products (**1b** + **1c**). [d] 3 mM substrate. [e] *E. coli* cells expressing P450 variant at OD_{600} = 40, 10 mM substrate, 50 mM potassium phosphate buffer (50 mM, pH 7.2), 16 hours.

Engineered XplA and BezE variants

To gain insights into the evolvability of these newly discovered C—H aminases, these P450s were subjected to mutagenesis. Upon inspection of the available crystal structure of XplA, residues Met322, Gln325, Val391, Met394, and Gln438 were found to project their respective side chains into the heme cavity where the sulfonyl azide substrate is expected to bind (**Figure 5b**). Accordingly, these positions were mutated to alanine with the two-fold purpose of expanding the active site volume and examining the impact of these mutations on XplA-dependent C—H aminase activity. While most of these mutations were found to reduce such activity, a two-fold improvement in the C—H amination activity of XplA was induced by the Q325A mutation (2,890 vs. 1,780 TTN; **Table 4**, Entries 3 vs. 1). Gln325 is located at the C-terminal end of the F-helix, 'gating' the entrance of the channel connecting the solvent to the heme pocket. Its mutation to alanine could thus potentially favor access of the bulky substrate **1a** to the heme cavity. We then tested the substitution of the conserved heme-ligating cysteine to serine (C503S), as an analogous mutation was found useful by the Arnold group to improve the nitrene transfer activity of $P450_{BM3}$.[18,20] This mutation proved beneficial toward increasing XplA C—H amination activity, resulting in a 210% increase in total turnovers for XplA-heme(C503S) vs. XplA-heme (3,830 vs. 1,780 TTN; Table 4, Entries 7 vs. 1). Finally, XplA was tested in the form of an artificial, catalytically self-sufficient system, where the heme domain of XplA is fused to the reductase domain of P450-RhF from *Rhodococcus* sp. NCIMB 9784[57-58], here referred to as 'XplA-RhF'.[59] This fusion construct, which resembles the multidomain arrangement of $P450_{BM3}$, was envisioned to allow for the reduction of XplA to the catalytically competent ferrous form by means of NADPH, thus enabling the use of this biocatalyst also in the context of whole-cell reactions. Notably, XplA-RhF showed a significantly improved C—H amination activity compared to XplA-heme, promoting the intramolecular C—H amination of **1a** with more than 4-fold higher TTN (8,090 vs. 1,780 TTN), along with improved selectivity (96% vs. 82%; **Table 4**, Entry 8 vs. 1). At a substrate loading of 3 mM, nearly quantitative conversion (>90%) of **1a** to **2a** was achieved using this enzyme in purified

form (Table 4, Entry 9). Furthermore, XplA-RhF could be applied to the biotransformation of **1a** into **2a** in whole cells, where it was determined to support over 13,400 turnovers (**Table 4**, Entry 10).

Despite the fact that BezE does not natively catalyze a monooxygenation reaction,[49] sequence alignment analysis of this enzyme against a diverse panel of P450s (**Figure S1**) suggests that it maintains the highly conserved proton relay threonine found in cytochromes P450, which corresponds to T256 in BezE primary sequence. Based on our results with the FL#62 variants, a T256V mutation was introduced in BezE to assess the effect of this substitution on the C—H amination activity of this P450. The resulting Bez(T256V) variant was found to exhibit slightly improved TTN for the cyclization of **1a** compared to the wild-type enzyme (11,200 vs. 10,800 TTN, Entry 13 vs. 12), along with a comparable rate of C—H amination (730 vs. 780 turnovers min^{-1}) and selectivity toward formation of the sultam product over the reduced byproduct (86% vs. 87%). Altogether, these studies demonstrated the robustness of both XplA and BezE to protein engineering toward further optimization of their nitrene transferase activity.

Kinetic Isotope Effect Experiments

Kinetic isotope effect (KIE) experiments were then performed to gain insights into the mechanism of these enzymes and effect of mutations. As summarized in **Table 5**, intermolecular kinetic isotope effects (KIE_{inter}) were estimated from comparison of the k_{cat} and k_{cat}/K_M values for the P450-catalyzed C—H amination reactions in the presence of non-deuterated azide **4a** and hexadeuterated azide **4a**-*d*$_6$, whereas the partially deuterated substrate **4a**-*d*$_3$ was utilized to assess the extent of intramolecular kinetic isotope effects (KIE_{intra}) in these transformations. For the FL#62-derived variants, these experiments yielded KIE_{inter} values close to or equal to unity (0.8-0.9 based on $(k_{cat})_{(H)}/(k_{cat})_{(D)}$; 0.6-0.8 based on $(k_{cat}/K_M)_{(H)}/(k_{cat}/K_M)_{(D)}$), whereas relatively large and positive KIE_{intra} ranging from 3.3 to 4.2 were measured for the intramolecular competition reactions (**Table 5**). Across this series of related variants, the intramolecular KIE values are thus consistently larger than those measured in the intermolecular settings and the KIE_{intra} increases with an increase of the enzyme's C—H amination activity. Comparison of KIE_{inter} vs. KIE_{intra} has proven useful to

examine rate-determining steps prior to the C—H bond cleaving step in catalytic mechanisms.[60-63] In the present system, the observation that $KIE_{inter} \approx 1$ (within experimental

Table 5. Inter- and intramolecular kinetic isotope effect experiments.[a]

a) Noncompetitive intermolecular KIE experiment (KIE_{inter}):

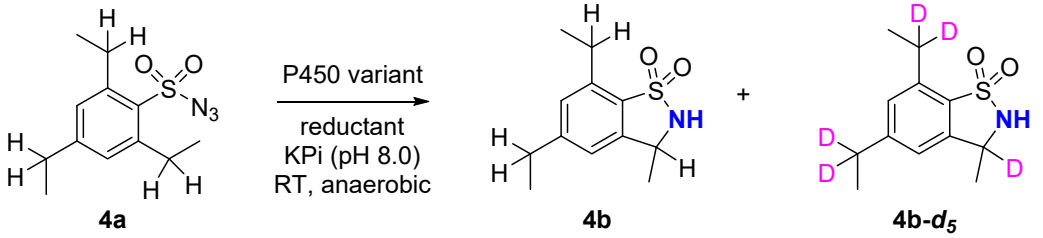

b) Competitive intermolecular KIE experiment (KIE_{inter}''):

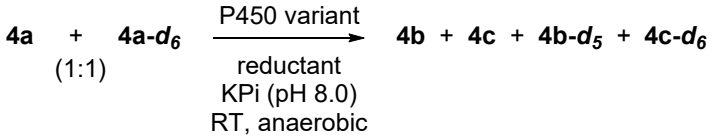

c) Intramolecular KIE experiment (KIE_{intra}):

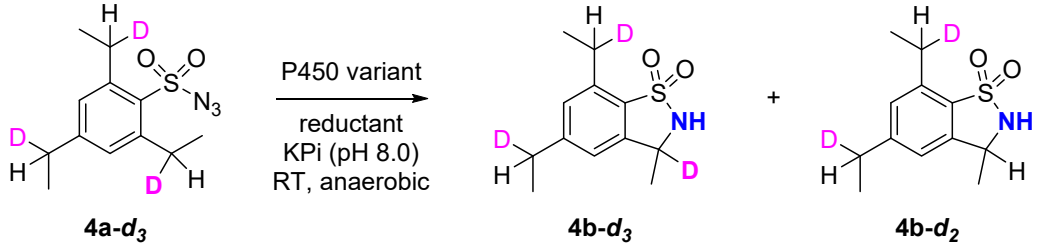

Variant	KIE_{inter} (k_{cat}(**4b**)/ k_{cat}(**4b-*d*5**))[b]	KIE_{inter} (k_{cat}/K_M(**4b**)/ k_{cat}/K_M(**4b-*d*5**))[b]	KIE_{intra} (**4b-*d*2:4b-*d*3**)	KIE_{inter}'' (**4b:4b-*d*5**)	KIE_{inter}'' (**4c:4c-*d*6**)
FL#62	0.9 ± 0.2	0.8 ± 0.2	3.3 ± 0.3	2.4 ± 0.3	0.5 ± 0.1
FL#62 (H266F,T268V)	0.8 ± 0.3	0.6 ± 0.1	4.1 ± 0.6	2.6 ± 0.1	0.4 ± 0.1

FL#62 (H266F,T268V,P392G)	0.9 ± 0.1	0.8 ± 0.2	4.2 ± 0.5	2.5 ± 0.1	0.7 ± 0.1
XplA-RhF	1.0 ± 0.2	0.9 ± 0.3	5.2 ± 0.1	2.0 ± 0.1	0.4 ± 0.1
BezE	0.2 ± 0.1	0.6 ± 0.2	3.7 ± 0.1	2.3 ± 0.1	1.0 ± 0.1

[a] 0.5 μM P450, 3 mM substrate(s), 10 mM reductant in 50 mM potassium phosphate buffer (pH 6.0 (BezE) or 8.0 (FL#62 and XplA variants)). [b] Corresponding k_{cat} and K_M values are provided in **Table S2**.

error) and that $KIE_{intra} >> KIE_{inter}$ suggests that a step prior to the C—H bond cleavage step is rate determining, resulting in 'masking' of the KIE associated with the latter.

Competitive intermolecular KIE experiments ($KIE_{inter''}$) were also carried out as these can provide complementary information compared to non-competitive intermolecular KIE experiments.[63] Under these conditions, $KIE_{inter''}$ values ranging from 2.4 to 2.6 were measured, which are consistently larger than the KIE_{inter} values measured under non-competitive settings. Further analysis of these intermolecular competition reactions revealed an inverse kinetic isotope effect ($KIE_{inter''}$ = 0.4-0.7) for the formation of the sulfonamide products **1c**, which showed an enrichment of the deuterated sulfonamide **4c**-*d*$_6$ over the protiated counterpart **4c**. Importantly, these $KIE_{inter''}$ values are approximately inversely proportional to the $KIE_{inter''}$ values measured based on the C—H amination products (i.e., **4b**/**4b**-*d*$_3$). Based on these results, the positive primary $KIE_{inter''}$ observed for the C—H amination reaction can be attributed to an induced kinetic isotope (IKIE) effect resulting from isotopically sensitive branching.[64-65] Induced kinetic isotope effects arise when two distinct products derive from a common reaction intermediate at a branching point in the catalytic mechanism.[64-69] Reasonably, as C—H amination is favored over C—D amination, reduction of the deuterated substrate can occur more readily, resulting in the accumulation of **4c**-*d*$_6$ over **4c** and thus in the observed inverse $KIE_{inter''}$ for the reduction product. Taking into account the contribution of the IKIE to the $KIE_{inter''}$, the 'true' KIE for these C—H amination reactions in the intermolecular H/D competition settings approaches the unity (i.e., $k_H/k_D \sim 1$), which is in agreement with the results from the non-competitive intermolecular KIE experiments. Given the significantly larger KIE observed in the intramolecular competition reaction (KIE_{intra} = 3.3-4.2) compared to KIE_{inter} and $KIE_{inter''}$ and the reasonable assumption that substrate binding to the enzyme is a significantly faster process compared to the overall rate of these reactions (4-13 turnovers min^{-1}), it can be derived that the

step(s) preceding the generation of the iron-nitrenoid intermediate, namely activation of the organic azide substrate (**Figure 1a**), is rate limiting in these reactions.

In the intramolecular competition experiments, the kinetic effects of the steps prior to C—H bond cleavage are eliminated due to formation of a common iron-nitrenoid intermediate. As such, the KIE_{intra} values directly report on the KIE associated with the C—H amination step. Under these conditions, the measured KIE_{intra} values of 3.3-4.2 (**Table 5**) are similar to those reported for the FL#62-catalyzed C—H amination of carbonazidates (KIE_{intra} = 4.7)[13] and [Ru(VI)(TMP)(NNs)$_2$]-catalyzed intermolecular C—H amination (k_H/k_D = 4.8; TMP = tetramethylporphyrin; Ns = -$SO_2C_6H_4NO_2$)[70]. Interestingly, the KIE_{intra} values for the improved FL62-based C—H aminases FL#62(H266F,T268V) and FL#62(H266F,T268V,P392G) (k_H/k_D = 4.1-4.2) are consistently higher than that of the parent enzyme FL#62 (k_H/k_D =3.3; **Table 5**). Insightfully, the magnitude of KIE_{intra} values in a mechanism with isotopically sensitive branching can be correlated to an increase in reaction rate for the formation of one product caused by reduction in the reaction rate for the generation of a second product.[67,71] In the present system, a reduction in the rate of the branching pathway leading to the reduction product is expected to make the rate of the overall reaction more dependent on the rate of the C—H amination step, resulting in an increase of the kinetic isotope effect associated with it. The increase in the KIE_{intra} values for the improved P450 variants is thus consistent overall with a suppression of the unproductive pathway as a result of the mutations targeted to the proton relay pathway and heme environment.

Interestingly, XplA and BezE were found to exhibit KIE_{inter}, $KIE_{inter''}$, and KIE_{intra} values of similar magnitude to those measured for the FL#62-derived variants as well as an analogous trend of the KIE_{inter} values being close to unity (0.6-0.9), $KIE_{inter''}$ being positive (2.0-2.3), and KIE_{intra} values (3.7-5.2) being larger than both KIE_{inter} and $KIE_{inter''}$ (**Table 5**). In addition, in analogy to the FL#62-derived variants, XplA-RhF showed an inverse kinetic isotope effect of 0.4 for formation of the sulfonamide product **1c**, indicating that the observed $KIE_{inter''}$ of 2.0 largely arises from an induced KIE. Considering the contribution of the latter to the $KIE_{inter''}$, the true KIE for the XplA-catalyzed intermolecular C—H amination reaction is close to one. This conclusion is consistent with the observed KIE_{inter} of 1.0 ± 0.3 obtained from the non-competitive intermolecular experiments. Given the

significantly larger KIE_{intra} of 5.2, it can be inferred that the azide activation step is rate limiting also in the XplA-catalyzed C—H amination reaction. In stark contrast, BezE showed a positive $KIE_{inter''}$ of 2.3 but no KIE for the formation of the reduction by-product, indicating the absence of a contribution from an IKIE to the $KIE_{inter''}$. Considering the KIE_{intra} of 3.7 measured for this enzyme, these results indicate the occurrence of only a partial masking of the KIE associated with the H/D substitution in the inter- vs. intramolecular competition reaction. In turn, these results suggest that in the BezE-catalyzed reaction the C—H amination step is kinetically competitive with the azide activation step.

Further Discussion

Taken together, the results described above contribute to depict a more detailed picture of the mechanism of P450-catalyzed C—H amination and they provide key insights into structural/functional features that control the efficiency and selectivity of P450s in these non-native reactions. First of all, the observation of the IKIE and associated isotopically sensitive branching in the $P450_{BM3}$- and XplA-catalyzed reactions corroborates the notion that the C—H amination product and reduction byproduct originate from the same catalytic intermediate. In turn, the present results provide, for the first time, experimental support to the proposed branching of the reaction pathway at the level of the iron-nitrenoid intermediate[12] as outlined in **Figure 1a**. Another important finding emerging from the present studies is that the initial activation of the azide substrate to generate the iron-nitrenoid intermediate (**Figure 1a**) is rate limiting in the P450-catalyzed C—H amination of sulfonyl azides. These findings should help contextualize previous claims concerning the C—H amination step being rate limiting in these reactions, which were done without considering the impact of IKIE deriving from isotopically sensitive branching on experimental $KIE_{inter''}$ values[15,21] and/or without considering the azide activation step in computational analyses of this reaction.[37] Interestingly, the rate limiting effect of the azide activation step in the present reactions is shared by C—H amination reactions with alkyl and aryl azides catalyzed by Co-[72] and Ru-porphyrins[73], but it diverges from the P450-catalyzed intramolecular C—H amination of carbonyl azides, in which the nitrene C—H insertion was determined to be rate limiting as suggested by comparably large $KIE_{inter''}$ (5.3) and KIE_{intra} (4.7)

values.[13] As such, our studies also highlight the impact of the type of nitrene precursor on affecting the kinetics of the catalytic steps involved in P450-catalyzed nitrene transfer.

Since the k_{cat}/K_M value describes the second order rate constant for the enzyme-catalyzed conversion of a substrate into a product, the increase in catalytic efficiency (k_{cat}/K_M: 56 → 280 $M^{-1}s^{-1}$, **Table 2**) across the series of engineered $P450_{BM3}$ variants can be interpreted on the basis of a beneficial effect of the introduced mutations toward accelerating these initial, rate determining steps of the catalytic cycle. Given the expected proximity of the heme-bound organic azide to the T268V residue in $P450_{BM3}$ active site (**Figure 2a**), we speculate that this residue may participate in stabilizing this complex (e.g., via H-bonding), thus contributing to a slowing down of the overall catalytic cycle. While for FL#62 and FL#62(H266F,T268V) most of the observed KIE_{inter}'' can be accounted for in terms of induced KIE, the true KIE estimated for the competitive intermolecular C—H amination reactions catalyzed by FL#62(H266F,T268V,P393G) remains positive (i.e., $k_H/k_D > 1$), suggesting that for this variant the C—H amination step becomes kinetically competitive with the azide activation step. In turn, this suggests that the azide activation step becomes faster in this P450 variant, which correlates with its overall faster C—H amination rate (i.e., 4- to 6-fold higher k_{cat}; **Table 2**) compared to FL#62 and FL#62(H266F,T268V). Interestingly, the behavior of FL#62(H266F,T268V,P393G) approaches that of BezE, which exhibits an even lower degree of 'masking' of the KIE for the inter- vs. intramolecular reaction as well as a faster C—H amination rate (k_{cat} = 14.7 s^{-1}; **Table 2**).

In line with our initial working hypothesis, disruption of the native proton relay system proved effective toward enhancing the catalytic activity of the $P450_{BM3}$-based C—H aminases. Our structure-activity data and mechanistic studies agree well in supporting the notion that such activity improvement is linked to a suppression of the unproductive (reductive) pathway, in particular in the context of substrates such as **4a**, in which this process is dominant over C—H amination. Our results show however that this beneficial effect is more general and not only—or not necessarily—associated with an increase in selectivity. Indeed, in the case of **1a**, in which C—H amination occurs with good selectivity, the mutations affecting the proton relay system induce a dramatic improvement in total turnovers (460 → 14,800 TTN), without having a significant impact on selectivity (87% vs. 86% for

FL#62; **Table 1**). These findings thus suggest a more complex mechanistic picture than originally anticipated (**Figure 1a**) and can be rationalized based on two possible, and not mutually exclusive, scenarios. Since an increase in TTN typically reflects a slower rate and/or fewer mechanisms of catalyst inactivation, a first hypothesis is that the rate enhancement induced by the mutations toward the productive C—H amination pathway more effectively outcompetes parallel and independent pathways leading to enzyme inactivation. In addition to the behavior of the improved FL#62-based variants, this scenario is generally consistent with the high TTN exhibited by XplA, which naturally lacks the proton relay network. Alternatively, the proton relay network may be *directly* implicated in these catalyst inactivation mechanisms. Consistent with either scenario, time-dependent analysis of the FL#62 reaction with **1a** revealed that degradation of the heme cofactor constitutes a major mechanism of biocatalyst inactivation during nitrene transfer catalysis and that this process proceeds more slowly in the FL#62(H266F,T268V) variant (**Figure S2**).

Finally, the present studies highlight the orthogonality of the structural requirements inherent to supporting high C—H amination reactivity compared to monooxygenase activity. This trend is particularly apparent across the series of $P450_{BM3}$ variants, where the progressive increase in C—H amination activity corresponds to a progressive loss in their monooxygenase activity (**Table 3**) and of the signature spectral features typical of P450s (**Figure 3**). In this regard, it is instructive to note that (*i*) the best performing $P450_{BM3}$-based C—H aminase, FL#62(H266F,T268V,P393G), has completely lost its P450-like features; and (*ii*) BezE shares with FL#62(H266F,T268V) and FL#62(H266F,T268V,P393G) the property of giving predominantly a 'P420 form' upon complexation with CO, thus indicating an altered heme environment compared to the canonical cytochrome P450 monooxygenases (**Figure 3**). Further supporting this point is the high C—H amination activity of XplA which features a non-canonical active site configuration and no observable monooxygenase activity toward **5**. Overall, whereas our results demonstrate that both XplA and BezE constitute highly promising and evolvable scaffolds for the development of new nitrene transferases, they also suggest that other natural P450s that naturally lack monooxygenase activity and/or other canonical P450-like structural features may constitute attractive platforms for this purpose.

Conclusions

In summary, this work demonstrates the value of mechanism-guided rational design as a strategy for developing and discovering new and efficient P450-based catalysts for C—H amination via nitrene transfer. Using this approach, engineered $P450_{BM3}$-based biocatalysts with dramatically enhanced catalytic turnovers, selectivity, and kinetics in the C—H amination of sulfonyl azides were obtained by targeting structural elements highly conserved across this family of enzymes. These studies revealed the divergent requirements associated with supporting nitrene transfer reactivity vs. monooxygenase activity, further leading to the identification of two 'atypical' natural P450s, XplA and BezE, as highly efficient C—H aminases. Both enzymes were amenable to further optimization of their C—H amination activity via protein engineering, thereby representing promising scaffolds, along with the engineered $P450_{BM3}$ variants, for the development of biocatalysts for nitrene transfer reactions and, possibly, other abiological transformations. Finally, characterization of these enzymes has yielded new and valuable insights into the mechanism of P450-catalyzed C—H amination and into structural/functional features that control the efficiency and selectivity of P450s in these non-native reactions. These findings are expected to prove useful toward guiding the future design and development of nitrene transferases based on hemoproteins and other metalloenzymes.

EXPERIMENTAL DETAILS

Reagents and Analytical Methods. All chemicals and reagents were purchased from commercial suppliers (Sigma-Aldrich, AlfaAesar, Chem-Impex, Fluka) and used without any further purification, unless otherwise stated. All moisture- or oxygen-sensitive reactions were carried out under an argon atmosphere in oven-dried glassware with magnetic stirring using standard gas-tight syringes, cannulae and septa. ^{1}H and ^{13}C NMR spectra were measured on a Bruker DPX-400 instrument (operating at 400 MHz for ^{1}H and 100 MHz for ^{13}C) or a Bruker DPX-500 instrument (operating at 500 MHz for ^{1}H and 125 MHz for ^{13}C). Tetramethylsilane (TMS) served as the internal standard (0 ppm) for ^{1}H NMR, $CDCl_3$ was used as the internal standard (77.0 ppm) for ^{13}C NMR. Silica gel chromatography purifications were carried out using AMD Silica Gel 60 Å 230-400 mesh. Thin Layer Chromatography (TLC) was carried out using Merck Millipore TLC silica gel

60 F254 glass plates. UV-Vis measurements were performed on a Shimadzu UV-2401PC UV-Vis spectrometer. HPLC analyses were performed on a Shimadzu LC-2010A-HT equipped with a VisionHT C18 reverse-phase column and a multidiode UV-Vis detector. Gas chromatography (GC) analyses were performed on a Shimadzu GC-2010 gas chromatograph equipped with a FID detector and a Chiral Cyclosil-B column (30 m x 0.25 mm x 0.25 μm). GC/MS analyses were performed on a Shimadzu GCMS-QP2010 equipped with a RTX-XLB column (30 m x 0.25 mm x 0.28 μm) and a quadrupole mass analyzer.

Cloning and Plasmid Construction. Compared to wild-type CYP102A1, FL#62 contains the following mutations: V78A, F81S, A82V, F87A, P142S, T175I, A180T, A184V, A197V, F205C, S226R, H236Q, E252G, R255S, A290V, L353V. The plasmid encoding FL#62(T268A) was prepared as described previously.[74] Vectors encoding the $P450_{BM3}$ variants with mutations to the proton relay system were prepared using pCWori_FL#62 as a template, primers BamHI_2_fwd and SacI_2_rev as superprimers, and the oligonucleotides of **Table S3** as mutagenizing primers. The target gene products (1.5 Kbp) were prepared by overlap extension (SOE) PCR, digested with *BamH* I and *Sac* I restriction enzymes, and ligated to *BamH* I/*Sac* I double-digested pCWori vector. Vectors encoding the $P450_{BM3}$ variants with mutations to the cysteine-heme-ligand loop were prepared using pCWori_FL#62(H266F,T268V) as a template, primers BamHI_2_fwd and BM3RedRev_short as megaprimers, and the oligonucleotides of **Table S3** as mutagenizing primers. The target gene products (3.2 Kbp) were prepared by stitching with overlap extension (SOE) PCR, digested with *BamH* I and *EcoR* I restriction enzymes, and ligated to *BamH* I/*EcoR* I double-digested pCWori vector. A LICRED-based vector encoding XplA-RhF[59] was kindly provided by Prof. Neal Bruce (University of York). Using this vector as template, genes encoding the XplA-heme variants were amplified by overlap extension (SOE) PCR using XplA_fw and XplA_rv as superprimers, and the oligonucleotides of **Table S3** as mutagenizing primers. The XplA-heme fragments were digested with *Nde* I and *Xho* I restriction enzymes and cloned into the *Nde* I/*Xho* I cassette of pET22b vector (Novagen). The vector encoding BezE was prepared using a synthetic DNA template (Genscript) with codons optimized for expression in *E. coli*. The bezE fragment was then amplified using the primers BezE_fw and BezE_rv, digested with *Nde* I and *Xho* I restriction enzymes and cloned into the *Nde* I/*Xho* I cassette of pET22b vector (Novagen).

Protein Expression and Purification. The $P450_{BM3}$ variants were expressed from pCWori-based plasmids containing the P450 gene under the control of a double tac promoter (*BamH* I/*EcoR* I cassette) as described previously.[74] Typically, cultures of recombinant DH5α cells in Terrific Broth (TB) medium containing ampicillin (100 mg L^{-1}) were grown at 37 °C (200 rpm) until OD_{600} reached 1.0 and then induced with 0.25 mM β-D-1-thiogalactopyranoside (IPTG) and 0.3 mM δ-aminolevulinic acid (ALA). After induction, cultures were shaken at 150 rpm and 27 °C and harvested after 20 hours by centrifugation at 3,400 x g at 4 °C. Cell lysates were prepared by sonication and loaded on Q resin. P450s were eluted using 20 mM Tris, 340 mM NaCl, pH 8.0. After buffer exchange (50 mM potassium phosphate buffer, pH 8.0), the enzymes were stored at -80 °C. The proteins XplA-heme, XplA-RhF and bezE were expressed and purified as reported previously.[49,53,59] P450 concentration was determined from CO-binding difference spectra ($\varepsilon_{450\text{-}490}$ = 91,000 M^{-1} cm^{-1}). For BezE and its T256V variant, concentration was determined based on their ferric form using ε_{420} = 101,000 M^{-1} cm^{-1} and 110,000 M^{-1} cm^{-1}, respectively, as determined using the hemochrome assay.[75] For FL#62(H266F,T268V) and FL#62(H266F,T268V,P393G), concentration was determined based on their ferric form using ε_{420} = 110,000 M^{-1} cm^{-1}, as determined using the hemochrome assay.[75] Phosphite dehydrogenase (PTDH) was expressed and purified as described previously.[74]

Enzymatic C—H Amination Reactions. The reactions using purified protein were carried out at 400 µL-scale using 0.5-1 µM P450, 3-10 mM substrate, and 10 mM NADPH in potassium phosphate buffer (50 mM, pH 8.0). In a typical procedure, a solution containing NADPH in potassium phosphate buffer (50 mM, pH 8.0) was degassed by bubbling argon into the mixture for 5 min in a sealed vial. A buffered solution containing the P450 enzyme was carefully degassed in a similar manner in a separate vial. The two solutions were then mixed together via cannulation. The reactions using *E. coli* whole cells expressing P450 variants were carried out at 400 µL-scale using 3-10 mM substrate, 50 mM glucose and 20 µL of an oxygen depletion system (from a stock solution containing 14,000 U/mL catalase and 1,000 U/mL glucose oxidase in 50 mM potassium phosphate buffer, pH 8.0). The cell suspension in 50 mM potassium phosphate buffer pH 7.2 and the glucose solution were carefully degassed by gentle sparging with argon for 40 and 10 min, respectively. In a typical procedure, 20 µL oxygen depletion system in a sealed vial was carefully degassed by purging the headspace with argon. Subsequently, cell suspension and glucose solution were added via syringe. Reactions were initiated by addition of 8 µL of azide (from a 0.5 M stock solution in

methanol) with a syringe, and the reaction mixture was stirred for 16 h at room temperature, under positive argon pressure. The reaction mixtures were analyzed by adding 8 μL of internal standard (fluorenone, 50 mM in DMSO) to the reaction mixture, followed by extraction with 400 μL of dichloromethane. The organic layer was removed via evaporation and the residue was dissolved in 300 μL methanol, filtered through 0.22 μm syringe filters, and analyzed by HPLC. Separation method: Injection volume: 20 μL. Flow rate: 1 mL/min. Gradient: 40% acetonitrile (0.1% TFA) in water (0.1% TFA) for 3 min, then increased to 90% over 15 min. Detector: 215 nm. Calibration curves were constructed using synthetically produced products. All measurements were performed at least in duplicate.

Michaelis-Menten Kinetic Analyses. Kinetic parameters for the intramolecular C—H amination reaction of 2,4,6-triisopropylbenzenesulfonyl azide **1a** were obtained from reactions carried out at the 0.5 mL-scale containing 1 μM purified P450, 10 mM NADPH in phosphate buffer (50 mM, pH 8.0) at room temperature. Azide **1a** concentration was varied (from 0.5 to 10 mM) and reactions were initiated by addition of the substrate. After 300 seconds, the samples were added with 1 mM fluorenone, extracted with dichloromethane, and analyzed by HPLC using calibration curves of authentic standards. The kinetic parameters V_{max}, k_{cat}, and K_M were obtained by non-linear fitting of the resulting plot of initial velocity (V) vs. substrate concentration to the Michaelis-Menten equation using SigmaPlot software. All measurements were performed at least in duplicates.

Hydroxylation Reactions. Analytical-scale reactions (1 mL) were carried out using 0.1-1 μM P450, 1 mM substrate, 2 μM PTDH, 100 μM $NADP^+$, and 50 mM sodium phosphite in phosphate buffer (50 mM, pH 8.0). After 16 hours at room temperature, the reaction mixtures were added with guaiacol (500 μM) as internal standard, extracted with dichloromethane, and analyzed by gas chromatography. Separation method: Injection volume: 1 μL. Injector temp.: 260 °C. Detector temp.: 260 °C. Gradient: column temperature set at 120 °C for 0 min, then to 150 °C at 17 °C min^{-1}, then to 240 °C at 10 °C min^{-1}. Total run time was 11.76 min.

Rate and Selectivity Analysis. Initial product formation rates were measured from 1 mL-scale reactions containing 0.5 mM substrate, 0.1-0.5 M purified P450, and 2 mM NADPH in phosphate buffer (50 mM, pH 8.0) at room temperature. After 30 seconds, the samples were added with 500 μM guaiacol and extracted with dichloromethane. Cofactor oxidation rate in the presence of

substrate was measured by monitoring NADPH depletion at 340 nm ($\varepsilon_{450\text{-}500}$ = 6.22 mM^{-1} cm^{-1}) using 0.1 - 0.5 μM purified P450, 0.5 mM substrate, and 200 μM NADPH. Selectivity was calculated from the ratio between the initial product formation rate and the initial NADPH oxidation rate.

Kinetic Isotope Effect Experiments. P450 reactions were carried out as above and stopped after 3 or 4 hours by extraction with dichloromethane. The organic solvent was evaporated, the residue taken up in 20 μL of CH_2Cl_2, and the products separated by preparative TLC (30% EtOAc in hexanes). The sultam product was collected from the TLC in 200 μL of CH_2Cl_2 and analyzed by GC/MS (see Reagents and Analytical Methods section). For the intramolecular KIE experiments (KIE_{intra}), 3 mM **4a**-*d3* was used and the KIE values were determined based on the ratios of the characteristic fragments with *m/z* of 227.1 (C—H amination) and 226.1 (C—D amination), as depicted in **Figure S3a**. For the competitive intermolecular KIE experiments ($KIE_{intra,}$), 1.5 mM each **4a** and **4a**-*d6* were used and the KIE values for sultam or sulfonamide production were determined based on the ratios of the characteristic fragments with *m/z* of 224.1 (non-deuterated) and 229.1 (deuterated), as depicted in **Figure S3b**. For the non-competitive KIE experiments (KIE_{inter}), Michaelis-Menten kinetic analyses were carried out using **4a** or **4a-*d_6*** at varying concentration (0.5 mM to 10 mM) in the presence of 5 μM P450 enzyme. Reactions were quenched after 10 min by extraction with dichloromethane and analyzed as described above. K_M and k_{cat} were derived via non-linear fitting of the initial velocity vs. substrate concentration plots to the Michaelis-Menten equation using SigmaPlot (**Table S2**) and KIE_{inter} were obtained from the ratios of the k_{cat} values (or k_{cat}/K_M values) in the presence of the protiated vs. deuterated substrate.

Synthetic Procedures. Sulfonyl azides **2a**, **3a** and **4a** were prepared according to previously reported procedures.[12] Authentic standards for sultams **1b**-**4b** were prepared using Co(TPP) as described previously.[12,76] (S)-ibuprofen methyl ester **5** was prepared as described previously.[31] The deuterated probe molecule 2,4,6-tris(ethyl-1,1-*d2*)benzenesulfonyl azide **4a-*d_6*** was synthesized as described in **Scheme S1** according to a reported procedure.[21] 2,4,6-Tris(ethyl-1-d)benzenesulfonyl azide **4a-*d_3*** were synthesized using an analogous procedure with the exception that $LiAlH_4$ was used instead of $LiAlD_4$ (**Scheme S1**).

1,3,5-Tris(1-bromoethyl-1-*d*)benzene (**9**). To a stirred solution of 1,3,5-triacetyl benzene (1 g, 4.9 mmol) in ethanol (15 mL) at 0 °C was added $NaBD_4$ (558 mg, 14.7 mmol). Upon completion

of the reaction (ca. 2 hours), the reaction mixture was quenched with water (1 mL) followed by extraction with ethyl acetate (3 × 10 mL). The combined organic layers were washed with brine, dried over Na_2SO_4 and evaporated under vacuum. The resulting alcohol **8** was used directly in next step without purification. To a stirred solution of **8** (991 mg, 4.65 mmol) in 30 mL CH_2Cl_2 at -5 °C was added PBr_3 (1 M in dichloromethane, 9.31 mmol) and the reaction was stirred for 12 h at room temperature. The reaction mixture was then poured in ice water followed by extraction with CH_2Cl_2 (3 × 15 mL). The combined organic layers were washed with brine, dried over Na_2SO_4, and evaporated under vacuum. Flash column chromatography of the obtained residue on silica gel furnished 1,3,5-tris(1-bromoethyl-1-*d*)-benzene **9** as colorless oil in 75% yield. R_f = 0.68 (1% EtOAc in hexanes). ^{1}H NMR (400 MHz, $CDCl_3$): δ 7.41 (s, 3H), 2.04 (s, 9H).

1,3,5-Tris(ethyl-1,1-*d*2)benzene (**10**). To a stirred solution of 1,3,5-tris(1-bromoethyl-1-d)benzene **9** (1.4 g, 3.5 mmol) in anhydrous tetrahydrofuran (25 mL) was added $LiAlD_4$ (880 mg, 21 mmol) at -20 °C. The temperature was slowly increased to room temperature, and the reaction mixture was then refluxed for 24 hours. Upon completion of the reaction, 10 mL ice-cold water was added dropwise to the reaction mixture on an ice-batch. The products were extracted with ether (2 × 50 mL). The organic phase was washed with water (3 × 50 mL), dried with anhydrous Na_2SO_4, and concentrated by evaporation. Flash chromatography purification on silica gel furnished 1,3,5-tris(ethyl-1,1-*d2*)benzene **10** as a colorless liquid in 15% yield. R_f = 0.88 (1% EtOAc in hexanes). ^{1}H NMR (400 MHz, $CDCl_3$): δ 6.98 (s, 3H), 1.22 (s, 9H). ^{13}C NMR (100 MHz, $CDCl_3$): δ 144.2, 124.8, 28.5–27.9, 15.9. GC–MS (*m/z*): 168 (M^+), 153 (M-CH_3), 137 (M-CH_3CD_2).

2,4,6-Tris(ethyl-1,1-*d*2)benzenesulfonyl azide (**4a-*d*$_6$**). To a stirred solution of 1,3,5-tris(ethyl-1,1-d2)benzene **10** (88 mg, 0.56 mmol) in anhydrous $CHCl_3$ (1 mL) at 0 °C under inert atmosphere was added $ClSO_3H$ (2.35 mmol) over 5 min. The reaction was stirred until completion of reaction as monitored by TLC. The reaction mixture was then poured into ice-cold water and extracted with dichloromethane (3 × 5 mL). The combined organic layers were washed with brine, dried over Na_2SO_4, and evaporated under reduced pressure to yield 2,4,6-tris(ethyl-1,1-d2)benzenesulfonyl chloride **11** as colorless oil (98% yield), which was carried out to the next step without further purification. To a stirred solution of 2,4,6-tris(ethyl-1,1-d2)benzenesulfonyl chloride **11** (136 mg, 0.51 mmol) in acetone/water (1:1) (3 mL) at 0 °C was added NaN_3 (66 mg, 1.03 mmol) and left

stirred at room temperature. After the reaction reached completion (~45 min), the reaction mixture was concentrated under reduced pressure, followed by extraction with dichloromethane (3 × 10 mL). The combined organic layers were washed with brine, dried over Na_2SO_4 and evaporated under reduced pressure. The residue was purified by flash chromatography on silica gel yielding 2,4,6-tris(ethyl-1,1-d2)benzenesulfonyl azide **4a**-*d*$_6$ in quantitative yield as a colorless oil. R_f = 0.61 (5% EtOAc in hexanes). ^{1}H NMR (400 MHz, $CDCl_3$): δ 7.06 (s, 2H), 1.27 (s, 6H), 1.24 (s, 3H). ^{13}C NMR (100 MHz, $CDCl_3$): δ 150.6, 146.3, 132.3, 129.6, 28.2–27.3, 16.6, 14.6. LC–MS (ESI) calculated for $C_{12}H_{11}D_6N_3NaO_2S$ $[M+Na]^+$ *m/z*: 297.3, Observed: 297.2.

2,4,6-Tris(ethyl-1-*d*)benzenesulfonyl azide (4a-*d*$_3$). Following the procedure for compound **11** and using **12** as starting material (**Scheme S1**), 2,4,6-tris(ethyl-1-*d*)benzenesulfonyl chloride **13** was isolated as yellow oil in 15% yield. R_f = 0.68 (in 5% EtOAc/hexane). ^{1}H NMR (400 MHz, $CDCl_3$): δ 7.09 (m, 2H), 3.3-3.11 (m, 2H), 2.66-2.64 (m, 1H), 3.81 (s, 3H), 1.31 (m, 6H), 1.25 (m, 3H). ^{13}C NMR (100 MHz, $CDCl_3$): δ 151.6, 145.7, 139.4, 130.0, 28.2, 16.1, 14.7. Following the procedure for compound **4a**-*d6* and using **13** as starting material, 2,4,6-tris(ethyl-1-*d*)benzenesulfonyl azide **4a**-*d3* was isolated as colorless oil in 92% yield. R_f = 0.66 (in 5% EtOAc/hexane). ^{1}H NMR (400 MHz, $CDCl_3$): δ 7.09-7.07 (m, 2H), 3.04 (m, 2H), 2.65 (m, 1H), 3.81 (s, 3H), 1.31-1.27 (m, 9H). ^{13}C NMR (100 MHz, $CDCl_3$): δ 150.7, 146.2, 132.2, 129.6, 28.1, 16.7, 14.7. LC–MS (ESI) calculated for $C_{12}H_{14}D_3N_3O_2S$ $[M+Na]^+$ *m/z*: 293.4, Observed: 293.5.

ASSOCIATED CONTENT

Supporting Information

Supporting information includes supplementary Tables and Figures, GC-MS spectra and HPLC chromatograms.

AUTHOR INFORMATION

ǂ These authors contributed equally to this work.

Corresponding Author:

* rfasan@ur.rochester.edu.

ACKNOWLEDGMENTS

This work was supported by the U.S. National Science Foundation grant CHE-1609550 and in part by the U.S. National Institute of Health (NIH) grant GM098628. The authors are grateful to Prof. Neal Bruce (University of York) for providing a plasmid for the expression of XplA and to Prof. Joseph Dinnocenzo (University Rochester) for helpful discussion about the KIE experiments. MS instrumentation was supported by the U.S. NSF grant CHE-0946653.

REFERENCES

(1) Dick, A. R.; Sanford, M. S. Transition Metal Catalyzed Oxidative Functionalization of Carbon—Hydrogen Bonds. *Tetrahedron* **2006**, *62*, 2439.

(2) Davies, H. M. L.; Manning, J. R. Catalytic C—H Functionalization by Metal Carbenoid and Nitrenoid Insertion. *Nature* **2008**, *451*, 417.

(3) Bruckl, T.; Baxter, R. D.; Ishihara, Y.; Baran, P. S. Innate and Guided C—H Functionalization Logic. *Acc. Chem. Res.* **2012**, *45*, 826.

(4) Hartwig, J. F.; Larsen, M. A. Undirected, Homogeneous C—H Bond Functionalization: Challenges and Opportunities. *ACS Cent. Sci.* **2016**, *2*, 281.

(5) Abrams, D. J.; Provencher, P. A.; Sorensen, E. J. Recent Applications of C—H Functionalization in Complex Natural Product Synthesis. *Chem. Soc. Rev.* **2018**, *47*, 8925.

(6) Muller, P.; Fruit, C. Enantioselective Catalytic Aziridinations and Asymmetric Nitrene Insertions into C—H Bonds. *Chem. Rev.* **2003**, *103*, 2905.

(7) Collet, F.; Dodd, R. H.; Dauban, P. Catalytic C—H Amination: Recent Progress and Future Directions. *Chem. Commun.* **2009**, 5061.

(8) Roizen, J. L.; Harvey, M. E.; Du Bois, J. Metal-Catalyzed Nitrogen-Atom Transfer Methods for the Oxidation of Aliphatic C—H Bonds. *Acc. Chem. Res.* **2012**, *45*, 911.

(9) Jeffrey, J. L.; Sarpong, R. Intramolecular C(sp3)—H Amination. *Chem. Sci.* **2013**, *4*, 4092.

(10) Driver, T. G. Recent Advances in Transition Metal-Catalyzed N-Atom Transfer Reactions of Azides. *Org. Biomol. Chem.* **2010**, *8*, 3831.

(11) Lu, H.; Zhang, X. P. Catalytic C—H Functionalization by Metalloporphyrins: Recent Developments and Future Directions. *Chem. Soc. Rev.* **2011**, *40*, 1899.

(12) Singh, R.; Bordeaux, M.; Fasan, R. P450-Catalyzed Intramolecular sp3 C—H Amination with Arylsulfonyl Azide Substrates. *ACS Catal.* **2014**, *4*, 546.

(13) Singh, R.; Kolev, J. N.; Sutera, P. A.; Fasan, R. Enzymatic C(sp(3))—H Amination: P450-Catalyzed Conversion of Carbonazidates into Oxazolidinones. *ACS Catal.* **2015**, *5*, 1685.

(14) Giovani, S.; Alwaseem, H.; Fasan, R. Aldehyde and Ketone Synthesis by P450-Catalyzed Oxidative Deamination of Alkyl Azides. *Chemcatchem* **2016**, *8*, 2609.

(15) Hyster, T. K.; Farwell, C. C.; Buller, A. R.; McIntosh, J. A.; Arnold, F. H. Enzyme-Controlled Nitrogen-Atom Transfer Enables Regiodivergent C—H Amination. *J. Am. Chem. Soc.* **2014**, *136*, 15505.

(16) Farwell, C. C.; McIntosh, J. A.; Hyster, T. K.; Wang, Z. J.; Arnold, F. H. Enantioselective Imidation of Sulfides via Enzyme-Catalyzed Intermolecular Nitrogen-Atom Transfer. *J. Am. Chem. Soc.* **2014**, *136*, 8766.

(17) Farwell, C. C.; Zhang, R. K.; McIntosh, J. A.; Hyster, T. K.; Arnold, F. H. Enantioselective Enzyme-Catalyzed Aziridination Enabled by Active-Site Evolution of a Cytochrome P450. *ACS Cent. Sci.* **2015**, *1*, 89.

(18) Prier, C. K.; Zhang, R. J. K.; Buller, A. R.; Brinkmann-Chen, S.; Arnold, F. H. Enantioselective, Intermolecular Benzylic C—H Amination Catalysed by an Engineered Iron-Haem Enzyme. *Nat. Chem.* **2017**, *9*, 629.

(19) Brandenberg, O. F.; Miller, D. C.; Markel, U.; Chaib, A. O.; Arnold, F. H. Engineering Chemoselectivity in Hemoprotein-Catalyzed Indole Amidation. *ACS Catal.* **2019**, *9*, 8271.

(20) Yang, Y.; Cho, I.; Qi, X. T.; Liu, P.; Arnold, F. H. An Enzymatic Platform for the Asymmetric Amination of Primary, Secondary and Tertiary C(sp(3))—H Bonds. *Nat. Chem.* **2019**, *11*, 987.

(21) Bordeaux, M.; Singh, R.; Fasan, R. Intramolecular C(sp(3))—H Amination of Arylsulfonyl Azides with Engineered and Artificial Myoglobin-Based Catalysts. *Bioorg. Med. Chem.* **2014**, *22*, 5697.

(22) Giovani, S.; Singh, R.; Fasan, R. Efficient Conversion of Primary Azides to Aldehydes Catalyzed by Active Site Variants of Myoglobin. *Chem. Sci.* **2016**, *7*, 234.

(23) Dydio, P.; Key, H. M.; Hayashi, H.; Clark, D. S.; Hartwig, J. F. Chemoselective, Enzymatic C—H Bond Amination Catalyzed by a Cytochrome P450 Containing an Ir(Me)-PIX Cofactor. *J. Am. Chem. Soc.* **2017**, *139*, 1750.

(24) Fasan, R.; Chen, M. M.; Crook, N. C.; Arnold, F. H. Engineered Alkane-Hydroxylating Cytochrome P450(BM3) Exhibiting Nativelike Catalytic Properties. *Angew. Chem. Int. Ed.* **2007**, *46*, 8414.

(25) Maurer, S. C.; Kuhnel, K.; Kaysser, L. A.; Eiben, S.; Schmid, R. D.; Urlacher, V. B. Catalytic Hydroxylation in Biphasic Systems Using CYP102A1 Mutants. *Adv. Synth. Catal.* **2005**, *347*, 1090.

(26) Kuehnel, K.; Maurer, S. C.; Galeyeva, Y.; Frey, W.; Laschat, S.; Urlacher, V. B. Hydroxylation of Dodecanoic Acid and (2R,4R,6R,8R)-Tetramethyldecanol on a Preparative Scale Using an NADH-Dependent CYP102A1 Mutant. *Adv. Synth. Cat.* **2007**, *349*, 1451.

(27) Chen, M. M.; Snow, C. D.; Vizcarra, C. L.; Mayo, S. L.; Arnold, F. H. Comparison of Random Mutagenesis and Semi-Rational Designed Libraries for Improved Cytochrome P450 BM3-Catalyzed Hydroxylation of Small Alkanes. *Protein Eng. Des. Sel.* **2012**, *25*, 171.

(28) Kolev, J. N.; O'Dwyer, K. M.; Jordan, C. T.; Fasan, R. Discovery of Potent Parthenolide-Based Antileukemic Agents Enabled by Late-Stage P450-Mediated C—H Functionalization. *ACS Chem. Biol.* **2014**, *9*, 164.

(29) Roiban, G. D.; Agudo, R.; Reetz, M. T. Cytochrome P450 Catalyzed Oxidative Hydroxylation of Achiral Organic Compounds with Simultaneous Creation of Two Chirality Centers in a Single C—H Activation Step. *Angew. Chem. Int. Ed.* **2014**, *53*, 8659.

(30) Venkataraman, H.; Verkade-Vreeker, M. C. A.; Capoferri, L.; Geerke, D. P.; Vermeulen, N. P. E.; Commandeur, J. N. M. Application of Engineered Cytochrome P450 Mutants as Biocatalysts for the Synthesis of Benzylic and Aromatic Metabolites of Fenamic Acid NSAIDs. *Bioorg. Med. Chem.* **2014**, *22*, 5613.

(31) Kolev, J. N.; Zaengle, J. M.; Ravikumar, R.; Fasan, R. Enhancing the Efficiency and Regioselectivity of P450 Oxidation Catalysts by Unnatural Amino Acid Mutagenesis. *Chembiochem* **2014**, *15*, 1001.

(32) Ren, X. K.; O'Hanlon, J. A.; Morris, M.; Robertson, J.; Wong, L. L. Synthesis of Imidazolidin-4-ones via a Cytochrome P450-Catalyzed Intramolecular C—H Amination. *ACS Catal.* **2016**, *6*, 6833.

(33) Shoji, O.; Yanagisawa, S.; Stanfield, J. K.; Suzuki, K.; Cong, Z. Q.; Sugimoto, H.; Shiro, Y.; Watanabe, Y. Direct Hydroxylation of Benzene to Phenol by Cytochrome P450BM3 Triggered by Amino Acid Derivatives. *Angew. Chem. Int. Ed.* **2017**, *56*, 10324.

(34) Sarkar, M. R.; Dasgupta, S.; Pyke, S. M.; Bell, S. G. Selective Biocatalytic Hydroxylation of Unactivated Methylene C—H Bonds in Cyclic Alkyl Substrates. *Chem. Commun. (Cambridge, U. K.)* **2019**, *55*, 5029.

(35) Ilie, A.; Harms, K.; Reetz, M. T. P450-Catalyzed Regio- and Stereoselective Oxidative Hydroxylation of 6-Iodotetralone: Preparative-Scale Synthesis of a Key Intermediate for Pd-Catalyzed Transformations. *J. Org. Chem.* **2018**, *83*, 7504.

(36) Strohmaier, S. J.; Huang, W. L.; Baek, J. M.; Hunter, D. J. B.; Gillam, E. M. J. Rational Evolution of the Cofactor-Binding Site of Cytochrome P450 Reductase Yields Variants with Increased Activity Towards Specific Cytochrome P450 Enzymes. *FEBS J.* **2019**, *286*, 4473.

(37) Li, Z.; Burnell, D. J.; Boyd, R. J. Computational Study of Engineered Cytochrome P450-Catalyzed C—H Amination: The Origin of the Regio- and Stereoselectivity. *J. Phys. Chem. B* **2017**, *121*, 10859.

(38) Denisov, I. G.; Makris, T. M.; Sligar, S. G.; Schlichting, I. Structure and Chemistry of Cytochrome P450. *Chem. Rev.* **2005**, *105*, 2253.

(39) Martinis, S. A.; Atkins, W. M.; Stayton, P. S.; Sligar, S. G. A Conserved Residue of Cytochrome P-450 Is Involved in Heme-Oxygen Stability and Activation. *J. Am. Chem. Soc.* **1989**, *111*, 9252.

(40) Raag, R.; Martinis, S. A.; Sligar, S. G.; Poulos, T. L. Crystal-Structure of the Cytochrome P-450cam Active-Site Mutant Thr252Ala. *Biochemistry* **1991**, *30*, 11420.

(41) Yeom, H.; Sligar, S. G.; Li, H.; Poulos, T. L.; Fulco, A. J. The Role of Thr268 in Oxygen Activation of Cytochrome P450BM-3. *Biochemistry* **1995**, *34*, 14733.

(42) Sevrioukova, I. F.; Li, H.; Zhang, H.; Peterson, J. A.; Poulos, T. L. Structure of a Cytochrome P450-Redox Partner Electron-Transfer Complex. *Proc. Natl. Acad. Sci. USA* **1999**, *96*, 1863.

(43) Vidakovic, M.; Sligar, S. G.; Li, H.; Poulos, T. L. Understanding the Role of the Essential Asp251 in Cytochrome P450cam Using Site-Directed Mutagenesis, Crystallography, and Kinetic Solvent Isotope Effect. *Biochemistry* **1998**, *37*, 9211.

(44) Martinis, S. A.; Blanke, S. R.; Hager, L. P.; Sligar, S. G.; Hoa, G. H.; Rux, J. J.; Dawson, J. H. Probing the Heme Iron Coordination Structure of Pressure-Induced Cytochrome P420cam. *Biochemistry* **1996**, *35*, 14530.

(45) Perera, R.; Sono, M.; Sigman, J. A.; Pfister, T. D.; Lu, Y.; Dawson, J. H. Neutral Thiol as a Proximal Ligand to Ferrous Heme Iron: Implications for Heme Proteins that Lose Cysteine Thiolate Ligation on Reduction. *Proc. Natl. Acad. Sci. USA* **2003**, *100*, 3641.

(46) Sun, Y.; Zeng, W.; Benabbas, A.; Ye, X.; Denisov, I.; Sligar, S. G.; Du, J.; Dawson, J. H.; Champion, P. M. Investigations of Heme Ligation and Ligand Switching in Cytochromes P450 and P420. *Biochemistry* **2013**, *52*, 5941.

(47) Rentmeister, A.; Arnold, F. H.; Fasan, R. Chemo-Enzymatic Fluorination of Unactivated Organic Compounds. *Nat. Chem. Biol.* **2009**, *5*, 26.

(48) Rylott, E. L.; Jackson, R. G.; Edwards, J.; Womack, G. L.; Seth-Smith, H. M. B.; Rathbone, D. A.; Strand, S. E.; Bruce, N. C. An Explosive-Degrading Cytochrome P450 Activity and its Targeted Application for the Phytoremediation of RDX. *Nat. Biotechnol.* **2006**, *24*, 216.

(49) Tsutsumi, H.; Katsuyama, Y.; Izumikawa, M.; Takagi, M.; Fujie, M.; Satoh, N.; Shin-Ya, K.; Ohnishi, Y. Unprecedented Cyclization Catalyzed by a Cytochrome P450 in Benzastatin Biosynthesis. *J. Am. Chem. Soc.* **2018**, *140*, 6631.

(50) Seth-Smith, H. M. B.; Rosser, S. J.; Basran, A.; Travis, E. R.; Dabbs, E. R.; Nicklin, S.; Bruce, N. C. Cloning, Sequencing, and Characterization of the Hexahydro-1,3,5-trinitro-1,3,5-

triazine Degradation Gene Cluster from Rhodococcus Rhodochrous. *Appl. Environ. Microb.* **2002**, *68*, 4764.

(51) Fournier, D.; Halasz, A.; Spain, J.; Fiurasek, P.; Hawari, J. Determination of Key Metabolites During Biodegradation of Hexahydro-1,3,5-trinitro-1,3,5-triazine with Rhodococcus sp Strain DN22. *Appl. Environ. Microb.* **2002**, *68*, 166.

(52) Jackson, R. G.; Rylott, E. L.; Fournier, D.; Hawari, J.; Bruce, N. C. Exploring the Biochemical Properties and Remediation Applications of the Unusual Explosive-Degrading P450 System XpIA/B. *Proc. Natl. Acad. Sci. USA* **2007**, *104*, 16822.

(53) Sabbadin, F.; Jackson, R.; Haider, K.; Tampi, G.; Turkenburg, J. P.; Hart, S.; Bruce, N. C.; Grogan, G. The 1.5-Angstrom Structure of XplA-heme, an Unusual Cytochrome P450 Heme Domain That Catalyzes Reductive Biotransformation of Royal Demolition Explosive. *J. Biol. Chem.* **2009**, *284*, 28467.

(54) Imai, T.; Globerman, H.; Gertner, J. M.; Kagawa, N.; Waterman, M. R. Expression and Purification of Functional Human 17 Alpha-Hydroxylase/17,20-Lyase (P450c17) in Escherichia Coli. *J. Biol. Chem.* **1993**, *268*, 19681.

(55) Yu, D. Y.; Xu, F. C.; Shao, L.; Zhan, J. X. A Specific Cytochrome P450 Hydroxylase in Herboxidiene Biosynthesis. *Bioorg. Med. Chem. Lett.* **2014**, *24*, 4511.

(56) Ding, Y.; Seufert, W. H.; Beck, Z. Q.; Sherman, D. H. Analysis of the Cryptophycin P450 Epoxidase Reveals Substrate Tolerance and Cooperativity. *J. Am. Chem. Soc.* **2008**, *130*, 5492.

(57) Roberts, G. A.; Celik, A.; Hunter, D. J. B.; Ost, T. W. B.; White, J. H.; Chapman, S. K.; Turner, N. J.; Flitsch, S. L. A Self-Sufficient Cytochrome P450 with a Primary Structural Organization that Includes a Flavin Domain and a [2Fe-2S] Redox Center. *J. Biol. Chem.* **2003**, *278*, 48914.

(58) Hunter, D. J. B.; Roberts, G. A.; Ost, T. W. B.; White, J. H.; Muller, S.; Turner, N. J.; Flitsch, S. L.; Chapman, S. K. Analysis of the Domain Properties of the Novel Cytochrome P450 RhF. *FEBS Lett.* **2005**, *579*, 2215.

(59) Sabbadin, F.; Hyde, R.; Robin, A.; Hilgarth, E. M.; Delenne, M.; Flitsch, S.; Turner, N.; Grogan, G.; Bruce, N. C. LICRED: A Versatile Drop-In Vector for Rapid Generation of Redox-Self-Sufficient Cytochrome P450s. *Chembiochem* **2010**, *11*, 987.

(60) Shearer, J.; Zhang, C. X.; Hatcher, L. Q.; Karlin, K. D. Distinguishing Rate-Limiting Electron Versus H-Atom Transfers in Cu-2(O-2)-Mediated Oxidative N-Dealkylations: Application of Inter- Versus Intramolecular Kinetic Isotope Effects. *J. Am. Chem. Soc.* **2003**, *125*, 12670.

(61) Jung, H. H.; Floreancig, P. E. Mechanistic Analysis of Oxidative C—H Cleavages Using Inter- and Intramolecular Kinetic Isotope Effects. *Tetrahedron* **2009**, *65*, 10830.

(62) Simmons, E. M.; Hartwig, J. F. On the Interpretation of Deuterium Kinetic Isotope Effects in C—H Bond Functionalizations by Transition-Metal Complexes. *Angew. Chem. Int. Ed.* **2012**, *51*, 3066.

(63) Guengerich, F. P. Kinetic Deuterium Isotope Effects in Cytochrome P450 Reactions. *Methods Enzymol.* **2017**, *596*, 217.

(64) Samuelson, A. G.; Carpenter, B. K. The Induced Kinetic Isotope Effect as a Tool for Mechanistic Discrimination. *J. Chem. Soc., Chem. Commun.* **1981**, 354.

(65) Jones, J. P.; Korzekwa, K. R.; Rettie, A. E.; Trager, W. F. Isotopically Sensitive Branching and Its Effect on the Observed Intramolecular Isotope Effects in Cytochrome P-450 Catalyzed-Reactions: A New Method for the Estimation of Intrinsic Isotope Effects. *J. Am. Chem. Soc.* **1986**, *108*, 7074.

(66) Croteau, R. B.; Wheeler, C. J.; Cane, D. E.; Ebert, R.; Ha, H. J. Isotopically Sensitive Branching in the Formation of Cyclic Monoterpenes - Proof That (-)-Alpha-Pinene and (-)-Beta-Pinene Are Synthesized by the Same Monoterpene Cyclase Via Deprotonation of a Common Intermediate. *Biochemistry* **1987**, *26*, 5383.

(67) Wagschal, K.; Savage, T. J.; Croteau, R. Isotopically Sensitive Branching as a Tool for Evaluating Multiple Product Formation by Monoterpene Cyclases. *Tetrahedron* **1991**, *47*, 5933.

(68) Cooper, H. L. R.; Mishra, G.; Huang, X. Y.; Pender-Cudlip, M.; Austin, R. N.; Shanklin, J.; Groves, J. T. Parallel and Competitive Pathways for Substrate Desaturation, Hydroxylation, and Radical Rearrangement by the Non-heme Diiron Hydroxylase AlkB. *J. Am. Chem. Soc.* **2012**, *134*, 20365.

(69) Gatto, N.; Vattekkatte, A.; Kollner, T.; Degenhardt, J.; Gershenzon, J.; Boland, W. Isotope Sensitive Branching and Kinetic Isotope Effects to Analyse Multiproduct Terpenoid Synthases from Zea mays. *Chem. Commun.* **2015**, *51*, 3797.

(70) Leung, S. K.; Tsui, W. M.; Huang, J. S.; Che, C. M.; Liang, J. L.; Zhu, N. Imido Transfer from Bis(imido)ruthenium(VI) Porphyrins to Hydrocarbons: Effect of Imido Substituents, C—H Bond Dissociation Energies, and Ru(VI/V) Reduction Potentials. *J. Am. Chem. Soc.* **2005**, *127*, 16629.

(71) Jacquot, C.; Wecksler, A. T.; McGinley, C. M.; Segraves, E. N.; Holman, T. R.; van der Donk, W. A. Isotope Sensitive Branching and Kinetic Isotope Effects in the Reaction of Deuterated Arachidonic Acids with Human 12- and 15-Lipoxygenases. *Biochemistry* **2008**, *47*, 7295.

(72) Kuijpers, P. F.; Tiekink, M. J.; Breukelaar, W. B.; Broere, D. L. J.; van Leest, N. P.; van der Vlugt, J. I.; Reek, J. N. H.; de Bruin, B. Cobalt-Porphyrin-Catalysed Intramolecular Ring-Closing

C-H Amination of Aliphatic Azides: A Nitrene-Radical Approach to Saturated Heterocycles. *Chem. - Eur. J.* **2017**, *23*, 7945.

(73) Manca, G.; Gallo, E.; Intrieri, D.; Mealli, C. DFT Mechanistic Proposal of the Ruthenium Porphyrin-Catalyzed Allylic Amination by Organic Azides. *ACS Catal.* **2014**, *4*, 823.

(74) Zhang, K.; El Damaty, S.; Fasan, R. P450 Fingerprinting Method for Rapid Discovery of Terpene Hydroxylating P450 Catalysts with Diversified Regioselectivity. *J. Am. Chem. Soc.* **2011**, *133*, 3242.

(75) Berry, E. A.; Trumpower, B. L. Simultaneous Determination of Hemes a, b, and c from Pyridine Hemochrome Apectra. *Anal. Biochem.* **1987**, *161*, 1.

(76) Ruppel, J. V.; Kamble, R. M.; Zhang, X. P. Cobalt-Catalyzed Intramolecular C—H Amination with Arylsulfonyl Azides. *Org. Lett.* **2007**, *9*, 4889.

Supporting Information for

Mechanism-Guided Design and Discovery of Efficient Cytochrome P450-Derived C—H Amination Biocatalysts

Viktoria Steck[‡], Joshua N. Kolev[‡], Xinkun Ren, and Rudi Fasan*

Department of Chemistry, University of Rochester, 14627 Rochester, New York, USA

‡ *Equal contribution.*

** Correspondence should be addressed to R.F. (rfasan@ur.rochester.edu)*

Table of contents:

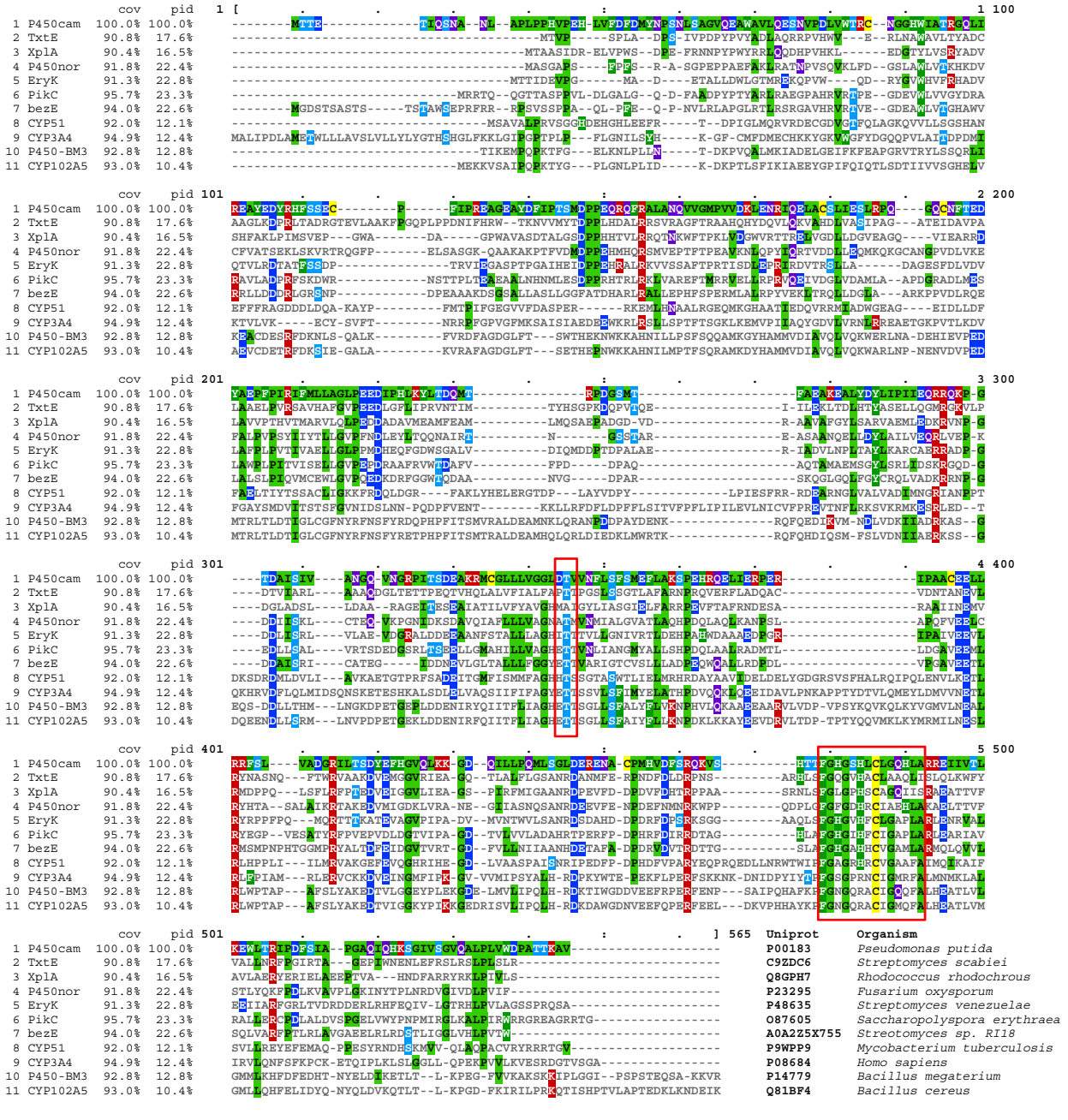

Figure S1. Multiple sequence alignment of P450$_{BM3}$, XplA, BezE and other cytochromes P450. The sequence alignment was constructed using the EMBL-EBI tool Clustal Omega[1] and formatted using MView.[2] Amino acid residues are color-coded by identity and query coverage (cov) and percent identity (pid) relative to the reference sequence P450$_{cam}$ are indicated. The regions

encompassing the conserved threonine residue and the heme-binding loop are highlighted with red boxes. Amino acid sequences (Uniprot) used are as follows: $P450_{cam}$, P00183, *Pseudomonas putida*; TxtE, C9ZDC6, *Streptomyces scabiei*; XplA, Q8GPH7, *Rhodococcus rhodochrous*; P450nor or CYP55A1, P23295, *Fusarium oxysporum*; P450 EryK or CYP113A1, P48635, *Saccharopolyspora erythraea*; P450 PikC or CYP107L1, O87605, *Streptomyces venezuelae*; bezE, A0A2Z5X755, *Streotomyces sp. RI18*; CYP51, P9WPP9, *Mycobacterium tuberculosis*; CYP3A4, P08684, *Homo sapiens*; $P450_{BM3}$ or CYP102A1, P14779, *Bacillus megaterium*; CYP102A5, Q81BF4, *Bacillus cereus*.

Figure S2. HPLC traces of a) hemin, b) heme extracted from FL#62, c) heme extracted from FL#62 incubated with $Na_2S_2O_4$, d) heme extracted from FL#62 reaction with 2,4,6-triisopropylbenzenesulfonyl azide **1a**, and e) heme extracted from FL#62(H266F,T268V) reaction with 2,4,6-triisopropylbenzenesulfonyl azide **1a**. Reaction conditions: Reactions were conducted as described in the Synthetic Procedures using 2 µM P450, with (c-e) or without 10 mM $Na_2S_2O_4$ (a-b), with (d-e) or without 10 mM **1a** (a-c), in 50 mM phosphate buffer (pH 7.0). After 10 minutes, the reaction mixture was extracted twice with 0.5 mL methyl ethyl ketone, and the combined organic layers removed under reduced pressure. The residue was dissolved in 100 µL methanol and analyzed by C18 RP-HPLC.

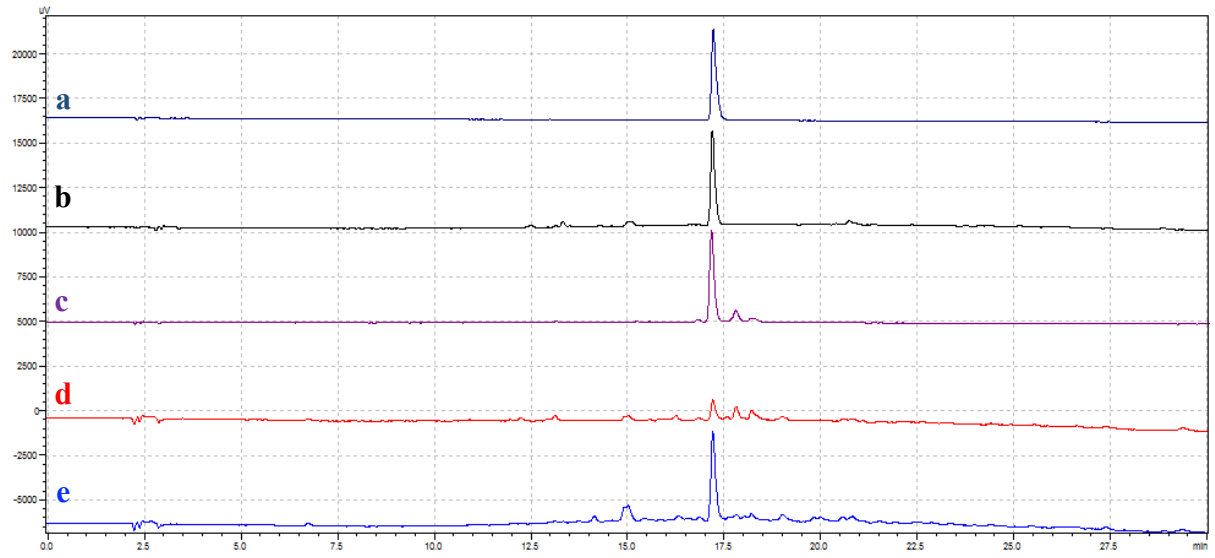

Figure S3. GC-MS traces and EI-MS spectra of products from the intra- and intermolecular H/D competition experiments. KIE values were obtained from integration of the MS signals corresponding to the characteristic fragmentation products with *m/z* of 227.1 (C—H amination) and 226.1 (C—D amination) for the intra-, and *m/z* of 224.1 (non-deuterated) and 229.1 (deuterated) for the intermolecular reaction. The insert boxes highlight the corresponding *m/z* values used for calculation of the KIE values.

a) GC-MS trace and EI-MS spectrum for P450-catalyzed intramolecular H/D competition reaction with **4a**-*d3*.

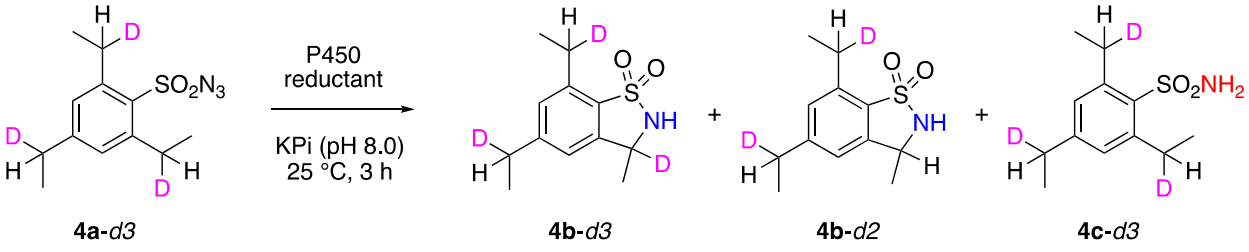

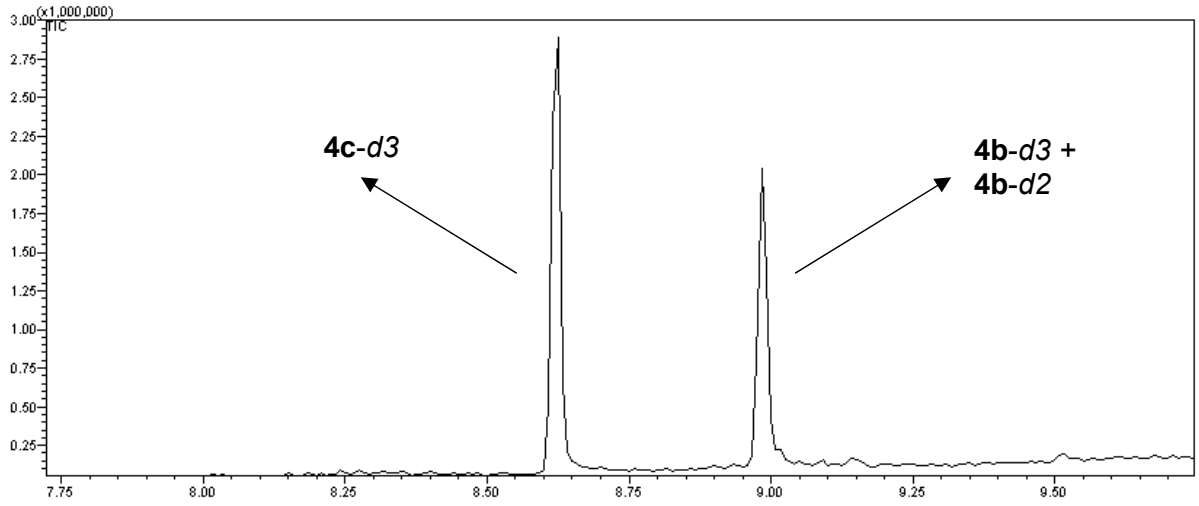

4b-*d3* + **4b**-*d2*:

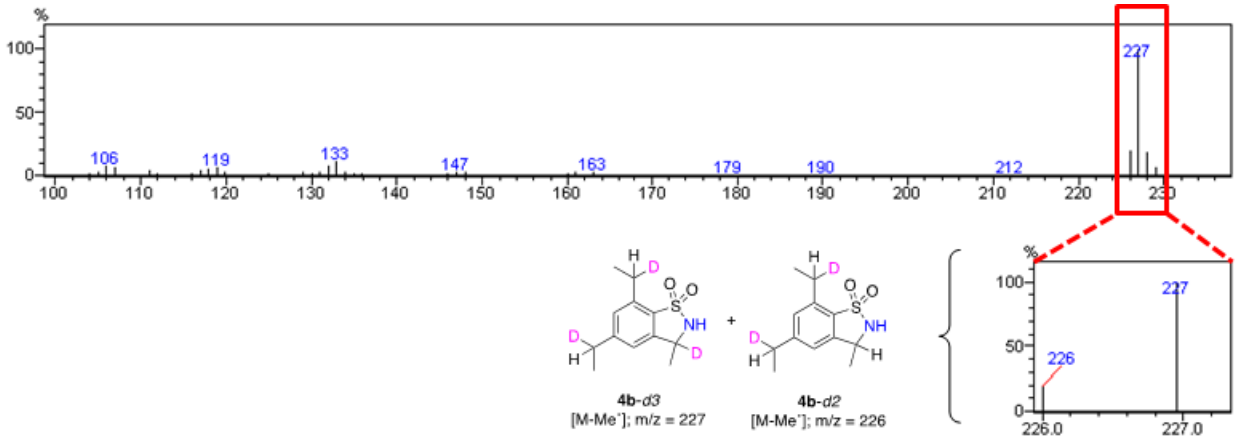

b) GC-MS trace and EI-MS spectra for P450-catalyzed intermolecular H/D competition reaction with **4a** and **4a**-*d6*.

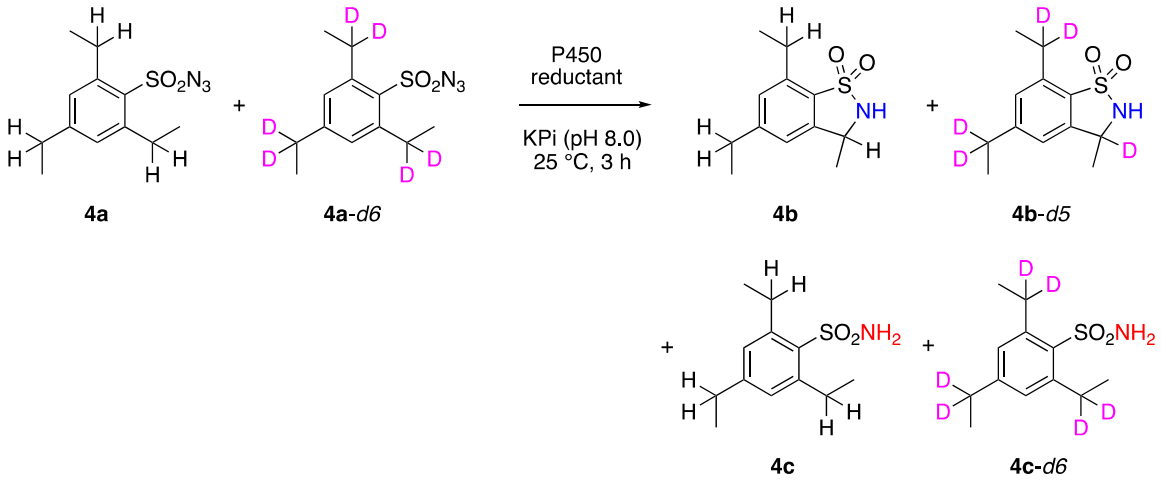

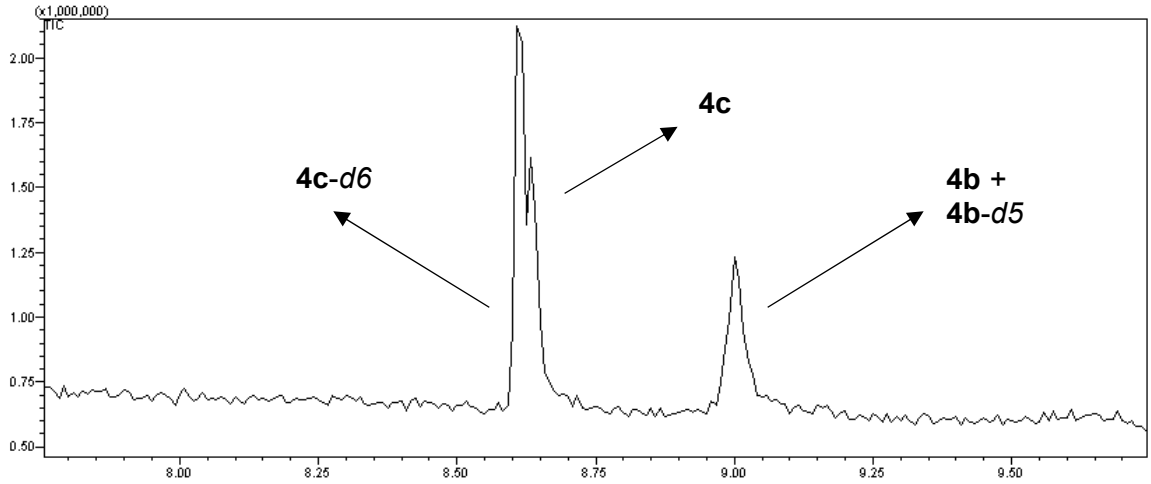

4c-*d6*:

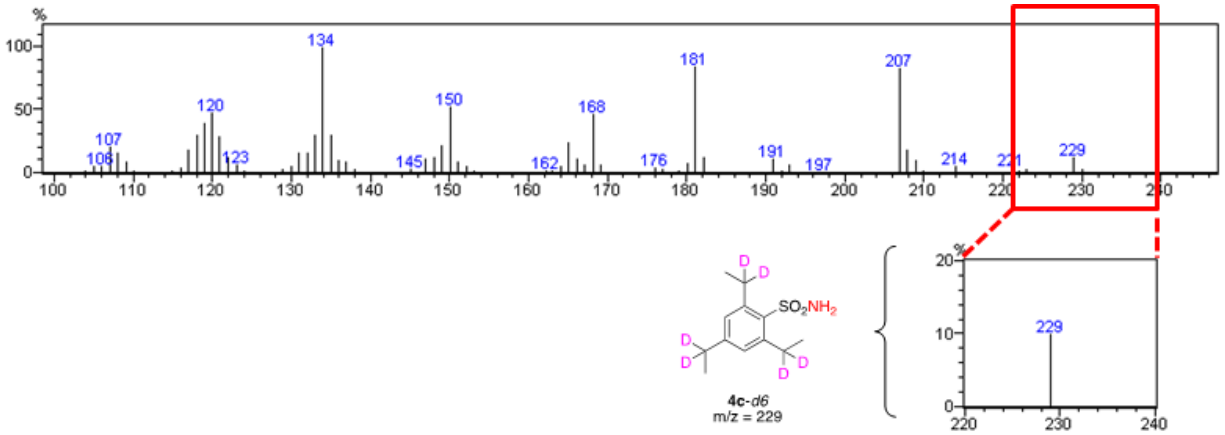

4c:

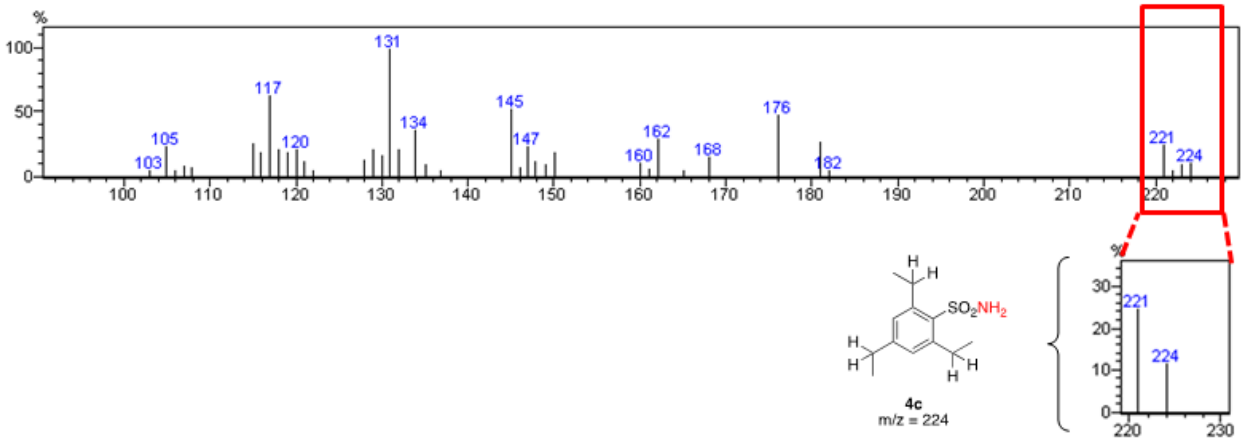

4b-*d3* + **4b**-*d2*:

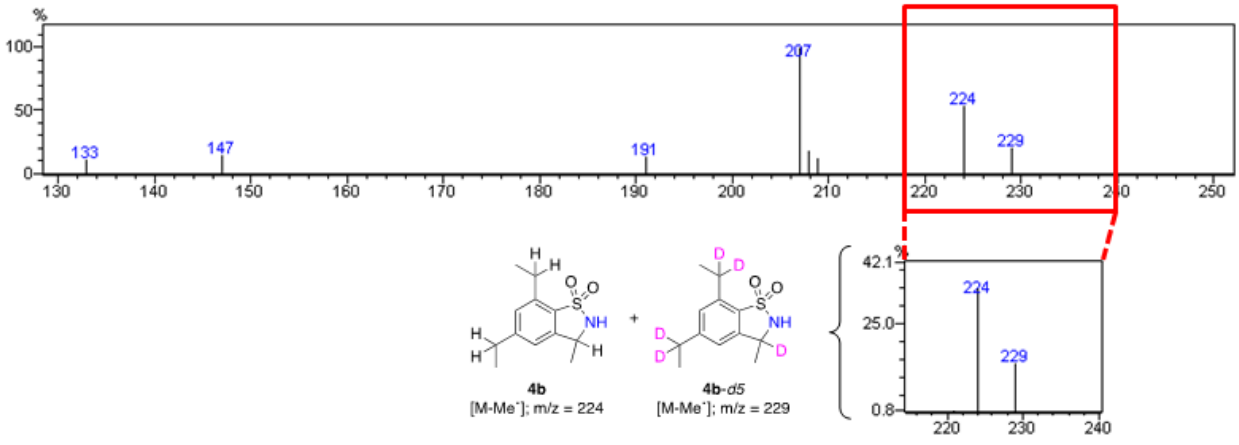

Table S1. Catalytic amination activity and selectivity of engineered P450$_{BM3}$ variants toward the C—H amination of 2,4,6-triethylbenzenesulfonyl azide **4a**.[a]

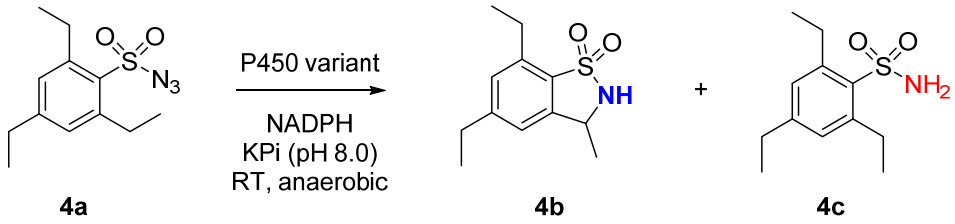

Entry	Variant	TTN[b]	Selectivity (%)[c]
1	FL#62	34 ± 4	17%
2	FL#62(H266F)	56 ± 5	21%
3	FL#62(E267A)	24 ± 4	8%
4	FL#62(T268A)	110 ± 5	21%
5	FL#62(T268V)	110 ± 15	28%
6	FL#62(T438V)	63 ± 20	15%
7	FL#62(H266F,T268V)	170 ± 25	28%
8	FL#62(E267A,T268V)	150 ± 10	23%
9	FL#62(E267A,T438V)	39 ± 12	11%
10	FL#62(T268V,T438V)	52 ± 5	29%
11	FL#62(H266F,T268V,T438V)	170 ± 15	31%
12	FL#62(H266F,T268V,P392G)	170 ± 25	14%
13	FL#62(H266F,T268V,F393P)	130 ± 10	10%
14	FL#62(H266F,T268V,G394P)	230 ± 25	9%
15	FL#62(H266F,T268V,I401P)	170 ± 12	26%
16	FL#62(H266F,T268V,G402P)	210 ± 15	10%

[a] 0.5 μM P450, 3 mM substrate, 10 mM NADPH, 50 mM KPi (pH 8.0), room temperature, anaerobic conditions.

[b] Total turnover numbers (mol sultam mol^{-1} P450).

[c] Mmol sultam (**4b**) / mmol total products (**4b** + **4c**).

Table S2. Noncompetitive intermolecular kinetic isotope effect experiments.[a]

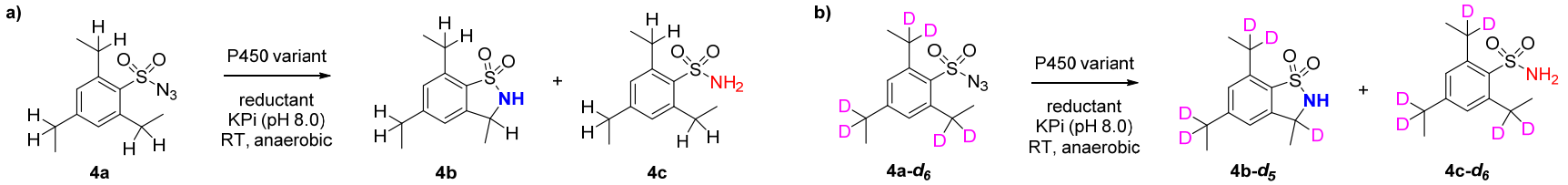

Variant	**4a** to **4b**[b]			**4a-*d*$_6$** to **4b-*d*$_5$**[b]		
	K_M (mM)	k_{cat} ($\times10^{-3}$ s^{-1})	k_{cat}/K_M ($M^{-1}s^{-1}$)	K_M (mM)	k_{cat} ($\times10^{-3}$ s^{-1})	k_{cat}/K_M ($M^{-1}s^{-1}$)
FL#62	5.1±0.3	39±2	7.6±0.6	4.3±0.6	43±5	10±1.8
FL#62 (H266F,T268V)	5.2±0.9	69±11	13±3	3.7±0.2	82±26	22±2
FL#62 (H266F,T268V,P392G)	0.41±0.09	2.8±0.1	6.8±1.6	0.35±0.01	3.0±0.4	8.6±1.2
XplA-RhF	0.72±0.03	45±11	62±15	0.60±0.08	44±2	73±10
BezE[c]	2.7±0.03	32±0.7	12±1.4	6.8±0.2	138±39	20±5.7

[a] Conditions: 5 µM P450, 0.5 mM to 10 mM substrate, 10 mM NADPH as reductant, 50 mM KPi buffer pH 8.0. Reactions were quenched at 10 min after addition of substrate. [b] K_M and k_{cat} values are estimated from Michaelis Menten equation; reported values are mean ± SD. [c] Using 10 mM $Na_2S_2O_4$ as reductant, 50 mM potassium phosphate buffer pH = 6.0.

Table S3. Sequence of the oligonucleotides in 5'-3' direction used for the preparation of engineered cytochrome P450 variants.

Entry	Primer	Sequence (from 5’ to 3’)
1	BamHI_2_fwd	GGAAACAGGATCCATCGATGC
2	SacI_2_rev	AATATCGAGCTCGTAGTTTGTATGATC
3	BM3RedRev_short	CGGGCTCAGATCTGCTCATG
4	FL#62_H266F_for	CTTAATTGCGGGATTTGAAACAAC
5	FL#62_H266F_rev	GTTGTTTCAAATCCCGCAATTAAG
6	FL#62_E267A_for	GGGACACGCGACAACAAGTG
7	FL#62_E267A_rev	CACTTGTTGTCGCGTGTCCC
8	FL#62_T268V_for	CGGGACACGAAGTGACAAGTGG
9	FL#62_T268V_rev	CCACTTGTCACTTCGTGTCCCG
10	FL#62_T438V_for	GATATTAAAGAAACTTTAGTGTTAAAACCTGAAG
11	FL#62_T438V_rev	CTTCAGGTTTTAACACTAAAGTTTCTTTAATATC
12	FL#62_E267A-T268V_for	GGGACACGCGGTGACAAGTG
13	FL#62_E267A-T268V_rev	CACTTGTCACCGCGTGTCCC
14	FL#62-P392G-for	GCGTTTAAAGGCTTTGGAAACG
15	FL#62-P392G-rev	CGTTTCCAAAGCCTTTAAACGC
16	FL#62-F393P-for	GTTTAAACCGCCGGGAAACG
17	FL#62-F393P-rev	CGTTTCCCGGCGGTTTAAAC
18	FL#62-G394P-for	CCGTTTCCGAACGGTCAGC
19	FL#62-G394P-rev	GCTGACCGTTCGGAAACGG
20	FL#62-I401P-for	GTGCGTGTCCGGGTCAGC
21	FL#62-I401P-rev	GCTGACCCGGACACGCAC
22	FL#62-G402P-for	CGTGTATCCCGCAGCAGTTC
23	FL#62-G402P-rev	GAACTGCTGCGGGATACACG
24	XplA_fw	CAGGTCATATGGGCTCGTCTCATCATCATCATCATC
25	XplA_rv	GGAACCTCGAGTTAGGACAGGACAATCGGCAGTTTA
26	XplA_M322A_fw	GTTATGGAAGCAATGTTTGAAGCTATGCTGGCGCAAAGCGCGGAAC
27	XplA_M322A_rv	GCTTCAAACATTGCTTCCATAAC

28	XplA_Q325A_fw	ATGGAAGCAATGTTTGAAGCTATGCTGATGGC GAGCGCGGAACCGG
29	XplA_Q325A_rv	ATAGCTTCAAACATTGCTTCCAT
30	XplA_V391A_fw	GCGATTGCCACGATCCTGGTGTTTTATGCAGCG GGCCACATGGCTA
31	XplA_V391A_rv	AACACCAGGATCGTGGCAATCGC
32	XplA_M394A_fw	ACGATCCTGGTGTTTTATGCAGTTGGCCACGCG GCTATTGGTTACC
33	XplA_M394A_rv	ACTGCATAAAACACCAGGATCGT
34	XplA_Q438A_fw	ATCAATGAAATGGTTCGTATGGACCCGCCGGCGCT GTCGTTTCTGC
35	XplA_Q438A_rv	TCCATACGAACCATTTCATTGAT
36	XplA_C503S_fw	AATCTGTCTTTTGGTCTGGGTCCGCACAGCAGCGCC GGTCAGATTA
37	XplA_C503S_rv	GGACCCAGACCAAAAGACAGATT
38	bezE_fw	ACACATCATATGGGCGATAGCACCAGCGC
39	bezE_rv	ACACATCTCGAGATTCCAGGTAACCGGCAGAT GAACC
40	bezE_T256V_fw	GTTTGGTGGCTATGAAGTGACCGTTGCG
41	bezE_T256V_rv	CGCAACGGTCACTTCATAGCCACCAAAC

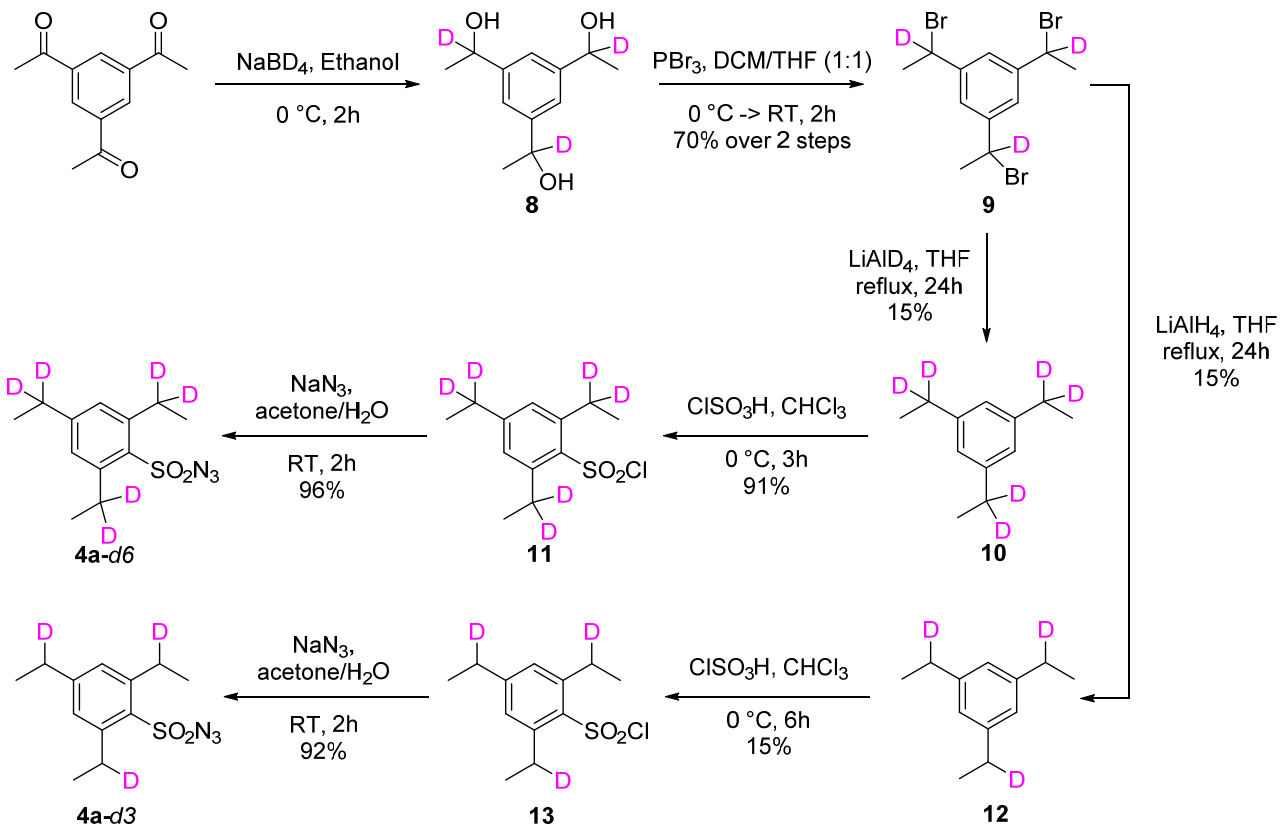

Scheme S1. Synthesis of the deuterated probe molecules 2,4,6-tris(ethyl-1,1-*d2*)benzenesulfonyl azide **4a**-*d6* and 2,4,6-tris(ethyl-1-d)benzenesulfonyl azide **4a**-*d3*.

References.

(1) Sievers, F.; Wilm, A.; Dineen, D.; Gibson, T. J.; Karplus, K.; Li, W.; Lopez, R.; McWilliam, H.; Remmert, M.; Söding, J.; Thompson, J. D.; Higgins, D. G. Fast, Scalable Generation of High-Quality Protein Multiple Sequence Alignments Using Clustal Omega. *Mol. Syst. Biol.* **2011**, *7*, 539.

(2) Brown, N. P.; Leroy, C.; Sander, C. MView: A Web-Compatible Database Search or Multiple Alignment Viewer. *Bioinformatics* **1998**, *14*, 380.